



1 **Underestimation of Column NO₂ Amounts from the OMI Satellite Compared to Diurnally**
2 **Varying Ground-Based Retrievals from Multiple Pandora Spectrometer Instruments**

3 Jay Herman¹, Nader Abuhassan¹, Jhoon Kim², Jae Kim³, Manvendra Dubey⁴, Marcelo Raponi⁵,
4 Maria Tzortziou⁶

5 **Abstract**

6 Retrievals of Total Column NO₂ (TCNO₂) are compared for 14 sites from the Ozone Measuring
7 Instrument (OMI using OMNO2-NASA v3.1) on the AURA satellite and from multiple ground-
8 based PANDORA spectrometer instruments making direct-sun measurements. Six of these sites
9 with multi-year PANDORA data records are in the Northern Hemisphere (Busan, Seoul,
10 Washington DC, Waterflow New Mexico, Boulder Colorado, and Mauna Loa) and one site in the
11 Southern Hemisphere (Buenos Aires Argentina). The first four of these sites and Buenos Aires
12 frequently have high TCNO₂ (TCNO₂ > 0.5 DU) and are likely have significant air quality problems
13 that can affect human health. Eight additional sites have shorter term data records in the US and
14 South Korea. One of these is a one-year data record from a highly polluted site at City College in
15 New York City with pollution levels comparable to Seoul, South Korea. The result is that on a
16 weekly or monthly average basis, OMI almost always underestimates the amount TCNO₂ by 50
17 to 100%, while occasionally the daily OMI value exceeds that measured by PANDORA at very
18 clean sites. OMI estimated air mass factor, surface reflectivity, and the OMI 24x13 km² FOV (field
19 of view) are three factors that can cause OMI to underestimate TCNO₂. Because of the local
20 inhomogeneity of NO₂ emissions, the large OMI FOV is the most likely factor when comparing
21 OMI TCNO₂ to retrievals from the small PANDORA effective FOV calculated from the solar
22 diameter of 0.5°. As part of air quality assessments, OMI always misses the frequently much
23 higher values of TCNO₂ that occur after the OMI overpass time.

24

25

Key Words: Nitrogen dioxide, OMI, PAN, PANDORA, ground-based, satellite

Correspondence email: jay.r.herman@nasa.gov

¹University of Maryland Baltimore County JCET, Maryland

²Department of Atmospheric Sciences, Yonsei National University, South Korea

³Department of Atmospheric Science, Pusan National University, South Korea

⁴Earth Systems Observations, Los Alamos National Laboratory, Los Alamos, NM 87545

⁵Departamento de Investigaciones en Láseres y Aplicaciones (DEILAP), Instituto de Investigaciones Científicas y Técnicas para la Defensa (CITEDEF), Ministerio de Defensa (MINDEF), Buenos Aires, Argentina

⁶City College of New York, New York City, NY



26 Underestimation of Column NO₂ Amounts from the OMI Satellite Compared to Ground-Based 27 Retrievals from Multiple Pandora Spectrometer Instruments

28 1.0 Introduction

29 Retrieval of Total Column NO₂ (TCNO₂) from the Ozone Monitoring Instrument (OMI) has been a
30 scientific success story for the past 14 years. Near total global coverage of the well-calibrated OMI has
31 enabled observation of all the regions where NO₂ is produced and has permitted monitoring of the
32 changes during the 2004 to 2019 period, especially in regions where there is heavy and growing industrial
33 activity (e.g., China and India). TCNO₂ amounts (data used: OMNO2-NASA v3.1) retrieved from OMI over
34 various specific land locations show a strong underestimate compared to co-located Pandora
35 Spectrometer Instruments (the abbreviation PAN is used for graph and table labels). The OMI TCNO₂
36 overpass time underestimate compared to ground-based measurements has been previously reported at
37 a few specific locations (Bechle, 2013; Lamsal et al., 2015; Ialongo et al., 2017; Kollonige, et al., 2018;
38 Goldberg et al., 2018; Herman et al., 2018). For any location, the OMI overpass local standard time consists
39 of the central overpass near the 13:30 hour equator crossing solar time and occasionally a side viewing
40 overpass from adjacent orbits within ±90 minutes of the central overpass time. Independently from
41 instrument calibration and retrieval errors, there are two specific aspects to the underestimation of TCNO₂
42 pollution levels. First, the mid-day OMI observations do not see the large diurnal variation of TCNO₂, and
43 second, the very large field of view (FOV) footprint 13 x 24 km² at OMI nadir view tends to average regions
44 of high pollution with those from lower pollution areas.

45 There are other possible systematic retrieval errors with OMI TCNO₂. The largest of these is
46 determining the air mass factor (AMF) needed to convert slant column measurements into vertical column
47 amounts. Accurately determining the AMF for TCNO₂ requires a-priori knowledge of the NO₂ profile shape
48 and using the correct surface reflectivity R_s. Currently R_s is found using a statistical process of sorting
49 through years of data to find relatively clear-sky scenes for each location (Kleipool, et al., 2008; O'Byrne
50 et al., 2010). Boersma et al., 2004 gave a detailed error analysis for the various components contributing
51 OMI TCNO₂ retrievals resulting an estimated "retrieval precision of 35-60%" in heavily polluted areas
52 dominated by determining the air mass factor. An improved V2.0 DOMINO retrieval (Boersma et al., 2011)
53 algorithm reduced the retrieval errors while increasing the estimated airmass factor, which reduces the
54 retrieved TCNO₂ up to 20% in winter and 10% in summer. The current version of OMNO2-NASA and v2.0
55 DOMINO are generally in good agreement (Marchenko et al., 2015; Zara et al., 2018). However, the
56 OMNO2-NASA retrievals are 10 to 15% lower than the v2.0 DOMINO retrievals. A subsequent detailed
57 analysis of surface reflectivity (Vasilkov et al., 2017) shows that retrieval of TCNO₂ in highly polluted areas
58 (e.g., some areas in China) can increase by 50% with the use of geometry-dependent reflectivities, but
59 only increase about 5% in less polluted areas. For PANDORA, calculation of the solar viewing AMF is a
60 simple geometric problem (AMF is approximately proportional to the cosecant of the solar zenith angle
61 SZA) and is independent of R_s (Herman et al., 2009). For a polluted region with TCNO₂ = 5.34x10¹⁶
62 molecules/cm² or 2 DU, the PANDORA error is expected to be about ±2.5% with the largest uncertainty
63 coming from an assumed amount of stratospheric TCNO₂ = 0.1 DU.



64 Accurate satellite TCNO₂ retrievals (and for other trace gases) are important in the estimate of
65 the effect of polluted air containing NO₂ on human health (Kim and Song, 2017 and references therein),
66 especially from the viewpoint of NO₂ as a respiratory irritant and precursor to cancer (Choudhari et al.,
67 2013). Since NO₂ is largely produced by combustion, satellite observations of NO₂ serve as a proxy for
68 changing industrial activity. Another important application requiring accurate measurements of the
69 amount of TCNO₂ and its diurnal variation is atmospheric NO₂ contribution to nitrification of coastal
70 waters (Tzortziou et al., 2018).

71 We show that the use of OMI TCNO₂ for estimating local air quality and coastal nitrification on a
72 global basis is misleading for most polluted locations, and especially on days when the morning or
73 afternoon amounts are higher than those occurring at the OMI overpass time near 13:30 hours standard
74 time. OMI TCNO₂ data are extremely useful for estimating regional pollution amounts and for assessing
75 long-term changes in these amounts. Modelling studies (Lamsal et al., 2017 Fig. 1) based on the Global
76 Modelling Initiative model (Strahan et al., 2007) simulating TCNO₂ diurnal variation over Maryland USA
77 (37-40°N, 74-79°W) shows a late afternoon peak and shows that the stratospheric component does not
78 substantially contribute to this peak. Boersma et al. (2016) show that sampling strategy can cause
79 systematic errors between OMI TCNO₂ and model TCNO₂ with satellite results being up to 20% lower than
80 models. Duncan et al., (2014) reviews the applicability of satellite TCNO₂ data to represent air quality and
81 notes that TCNO₂ correlates well with surface levels of NO₂ in industrial regions and states that the portion
82 of TCNO₂ in the boundary layer could be over 75% of the total vertical column depending on NO₂ altitude
83 profile shape.

84 This paper presents 14 comparisons between retrieved OMI TCNO₂ overpass values that are co-
85 located with PANDORA TCNO₂ amounts from various locations in the world. Six of the comparisons are
86 where PANDORAs have long-term data (1-year or longer) records. The comparisons are done using daily
87 data matched to the OMI overpass times ±6 minutes and with monthly running averages calculated using
88 Lowess(f) (Locally Weighted least squares fit to a fraction f of the data points, (Cleveland, 1981)) of time
89 matched TCNO₂. This is combined with a discussion and presentation of data on the effect of diurnal
90 variation that are always missed at the local OMI mid-day overpass times. We show that OMI TCNO₂
91 values are systematically lower than PANDORA values at sites with significant pollution (TCNO₂ > 0.3 DU).
92 We also present a unique view of a year of daily diurnal variation of TCNO₂ at two sites, Washington DC
93 and New York City, which are similar to other polluted locations.

94

95 **2.0 Brief Instrument Descriptions**

96 For the purposes of TCNO₂ retrievals, both OMI and PANDORA are spectrometer-based
97 instruments using nearly the same spectral range and similar spectral resolution (about 0.5 nm). Both use
98 spectral fitting retrieval algorithms that differ (Boersma et al. 2011; Herman et al., 2009) because of the
99 differences between direct-sun viewing retrievals (PANDORA) and above the atmosphere downward
100 viewing retrievals (OMI). The biggest difference is with the respective fields of view, 13 x 24 km² at OMI
101 nadir view and larger off-nadir FOV compared to the much smaller PANDORA FOV (1.2°) measured in m²
102 with the precise value depending on the NO₂ profile shape and the solar zenith angle. For example, if most



103 of the TCNO₂ is located below 2 km, then the PANDORA FOV is approximately given by
104 $(1.2\pi/180)(2/\cos(\text{SZA}))$, which for SZA = 45° is about 59x59 m².

105 2.1 OMI

106 OMI is an east-west side (2600 km) and nadir viewing polar orbiting imaging spectrometer that
107 measures the earth's backscattered and reflected radiation in the range 270 to 500 nm with a spectral
108 resolution of 0.5 nm. The polar orbiting side scanning capabilities produce a pole to pole swath that is
109 about 2600 km wide displaced in longitude every 90 minutes by the earth's rotation to provide coverage
110 of nearly the entire sunlit Earth once per day at a 13:30 solar hour equator crossing time with spatial gaps
111 at low latitudes. OMI provides full global coverage every 2 to 3 days. Additional gaps are caused by a
112 problem with the OMI CCD, "row anomaly" (Torres et al., 2018) that effectively reduces the number of
113 near-nadir overpass views. A detailed OMI instrument description is given in Levelt et al. (2006). TCNO₂ is
114 determined in the visible spectral range from 405 to 465 nm where the NO₂ absorption spectrum has the
115 maximum spectral structure and where there is little interference from other trace gas species (there is a
116 weak water feature in this range). OMI overpass data are available for many sites (currently 719) from the
117 following NASA website. <https://avdc.gsfc.nasa.gov/index.php?site=666843934&id=13>

118

119 2.2 PANDORA

120

121 PANDORA is a sun-viewing instrument for SZA < 80° that obtains about 4000 spectra for clear-sky
122 views of the sun in 20 seconds for each of two ranges UV (290 – 380 nm using a UV340 bandpass filter)
123 and visible plus UV (280 – 525 nm using no filter). The overall measurement time is about 80 seconds
124 including a 20 second dark-current measurements between each spectral measurement throughout the
125 day. About 4000 clear-sky spectra for the UV and visible portions are separately averaged together to
126 achieve very high signal to noise ratios (SNR). The UV340 filter for UV portion of the spectra reduces stray
127 light effects from the visible wavelength range. A detailed description of PANDORA and its SNR is given
128 in Herman et al., (2009; 2015). The effect of moderate cloud cover (reduction of observed signal by a
129 factor of 8) in the PANDORA FOV on TCNO₂ retrievals is small (Herman et al., 2018). Cloud cover also
130 reduces the number of measurements possible in 20 seconds, which potentially increases the noise level.
131 PANDORA is driven by a highly accurate sun tracker that points an optical head at the sun and transmits
132 the received light to an Avantes 2048 x 32 pixel CCD spectrometer (AvaSpec-ULS2048 from 280 – 525 nm
133 with 0.6 nm resolution) through a 50 micron diameter fiber optic cable. The estimated TCNO₂ error is
134 approximately 0.05 DU (1 DU = 2.69 x 10¹⁶ molecules cm⁻²) out of a typical value of 0.3 DU in relatively
135 clean areas and over 3 DU in highly polluted areas. PANDORA data are available for 250 sites. Some sites
136 have multi-year data sets, but many of these sites are short-term
137 campaign sites. https://avdc.gsfc.nasa.gov/pub/DSCOVER/Pandora/DATA_01/.

138

139 3.0 Overpass Comparisons and Diurnal Variation of TCNO₂

140

141 NO₂'s contribution to air quality at the Earth's surface is usually a proportional function of TCNO₂
142 that varies with the time of day and with the altitude profile shape. Most of the NO₂ amount is usually



143 located between 0 and 3 km altitude with a small amount (about 0.1 DU) in the upper troposphere and
144 stratosphere. Because of the relatively short chemical lifetime, 3-4 hours (Liu et al., 2016), in the lower
145 atmosphere, most of the NO₂ is located near (0 to 20 km) its sources (industrial activity, power generation,
146 and automobile traffic). At higher altitudes or in the winter months, the life time of NO₂ is longer
147 permitting transport over larger distances from its sources.

148

149 During the South Korean campaign (KORUS-AQ) in the spring of 2016 the diurnal variations of
150 TCNO₂ vs days of the year DOY were determined for 6 sites (Herman et al., 2018), one of which is
151 reproduced here (Fig. 1) for the city of Busan showing relatively low values of TCNO₂ in the morning (0.5
152 DU), moderately high values during the middle of the day (1.3 DU), and very high values in the afternoon
153 (2 to 3 DU). Of these data, OMI only observes midday values near the 13:30 time marked on the Local
154 Time axis of Fig.1 thereby missing very high values (2 to 3 DU) that frequently occur later in the afternoon
155 coinciding with times when people are outdoors returning from work.

156

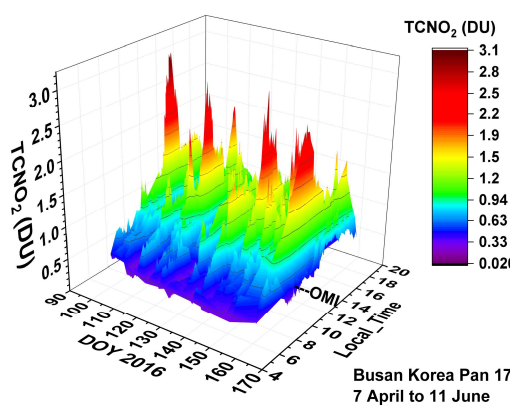


Fig 1 Diurnal variation of TCNO₂ measured at Pusan University in Busan South Korea

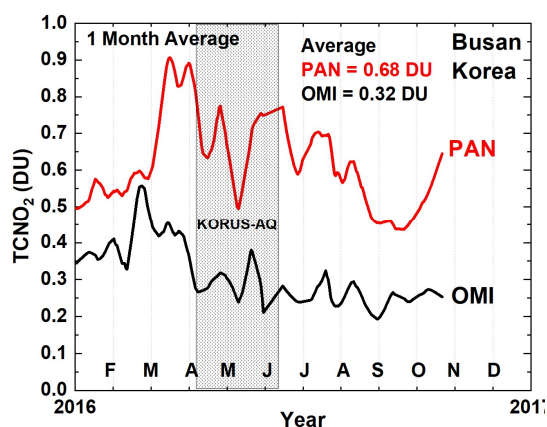


Fig. 2. Monthly average values of TCNO₂ for OMI and PANDORA at OMI overpass times

157

158 In addition to missing the TCNO₂ diurnal variation, the OMI values are about half those observed
159 by PANDORA (Fig. 2) at the OMI overpass time, so that using OMI values to estimate NO₂ pollution
160 seriously underestimates the air quality problem even at midday. The shaded area in Fig.2 corresponds to
161 the period covered in the KORUS-AQ campaign 7 April to 11 June 2016 shown in Fig. 1. An extended time
162 series for Busan location is shown in Fig. 3.

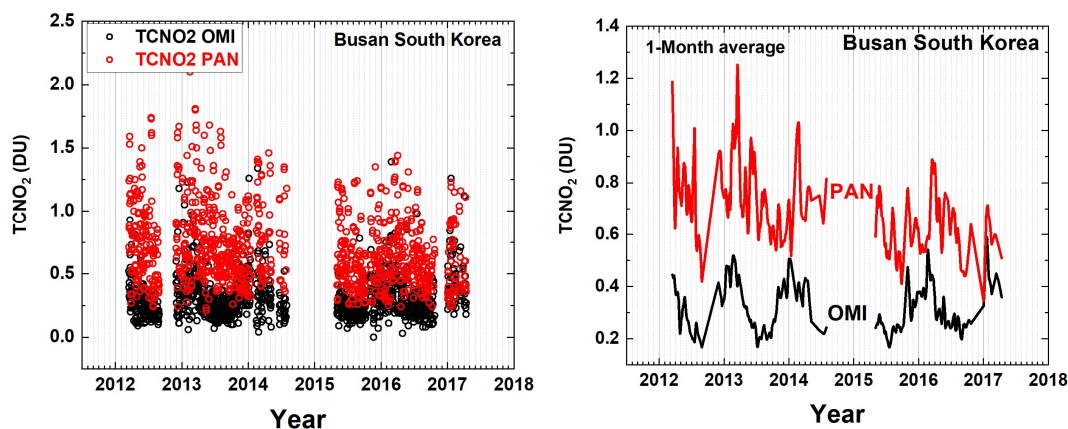


Fig. 3 Extended time series for Busan. Left Panel: individual matching PANDORA and OMI data points for the overpass time ± 6 minutes. Right Panel: monthly averages.

163

164

165

166

167

168

169

170

171

172

173

174

175

176

177

178

179

180

181

182

183

184

185

Because of the different effective NO_2 FOV of PANDORA (measured in meters²) while tracking the moving sun position located in the heart of Busan (FOV distance $d < 5$ km for an $\text{SZA} < 70^\circ$ used for TCNO_2 retrievals), both the daily (Fig. 3, left panel) and PANDORA monthly average variation (Fig. 3, right panel), obtained at the OMI overpass time, differs from the variation in the OMI TCNO_2 because of the much larger OMI FOV (13×24 km² at OMI nadir view) retrieval. Because of this, the OMI time series has low correlation ($r^2 = 0.1$) with the PANDORA time series.

The extended OMI vs PANDORA time series from 2012 – 2017 for Busan (Fig. 3) shows the same magnitude of differences seen during the KORUS-AQ period. A similar OMI vs PANDORA plot for total column ozone TCO_3 (Appendix Fig A1) shows good agreement between PANDORA and OMI indicating that the PANDORA instrument was operating and tracking the sun properly. Because the spatial variability of TCO_3 , which is mostly in the stratosphere, is much less than for TCNO_2 , the effect of different FOV's is minimized.

The same type of differences, $\text{TCNO}_2(\text{PAN}) > \text{TCNO}_2(\text{OMI})$, are seen at a wide variety of sites (e.g., see Fig.4). Comparing extended Busan multi-year time series, some broad-scale correlation can be seen with peaks in February 2013, January 2014, and in 2016. The data from Busan are different than from many sites, since Busan is located very near the ocean causing a portion of the OMI FOV to be over the unpolluted ocean areas, whereas PANDORA is located inland in an area of dense automobile traffic and quite near mountains capable of trapping air.

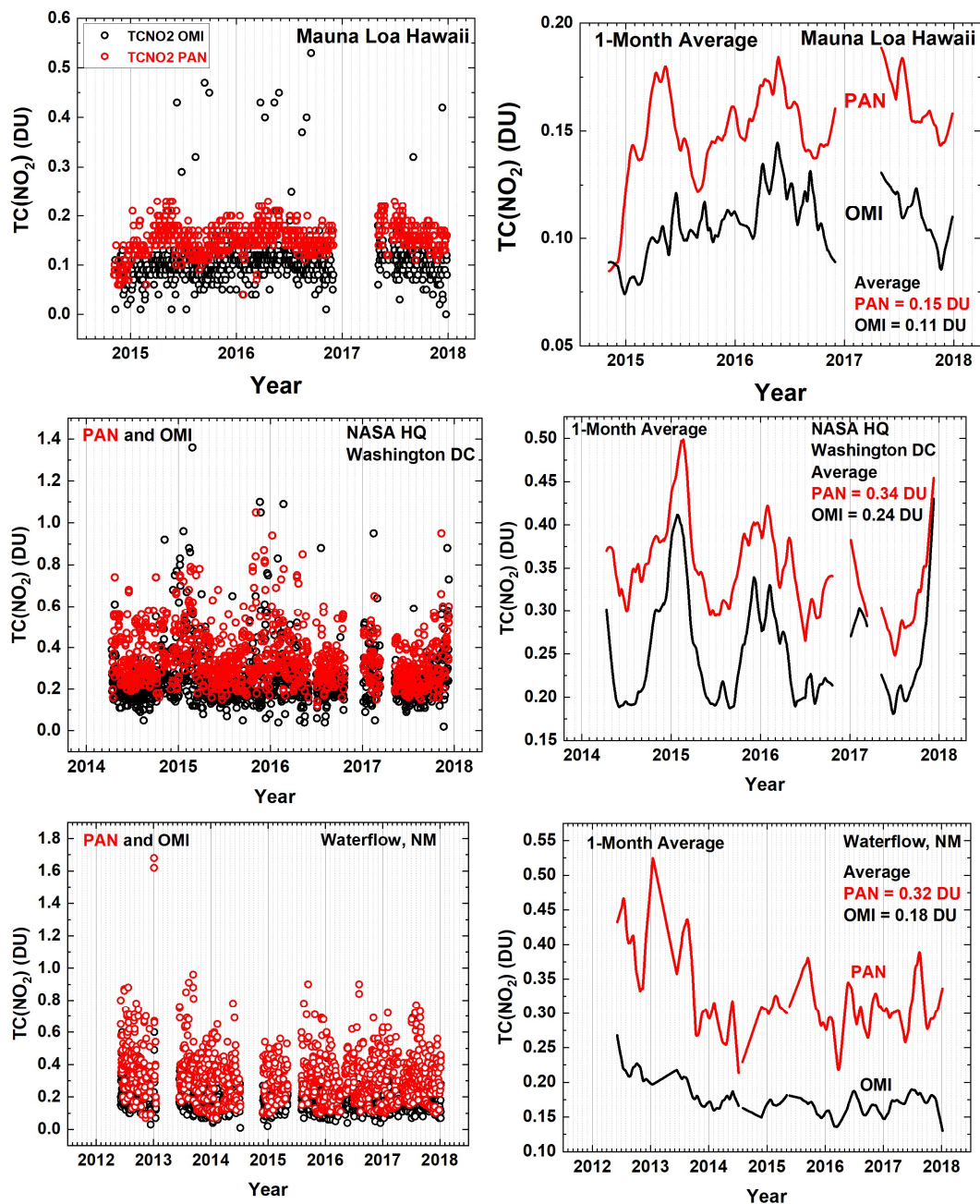


Fig. 4. PANDORA compared to OMI. Extended TCNO₂ overpass time series for Mauna Loa Observatory, Hawaii, NASA Headquarters, Washington DC, and Waterflow, New Mexico.

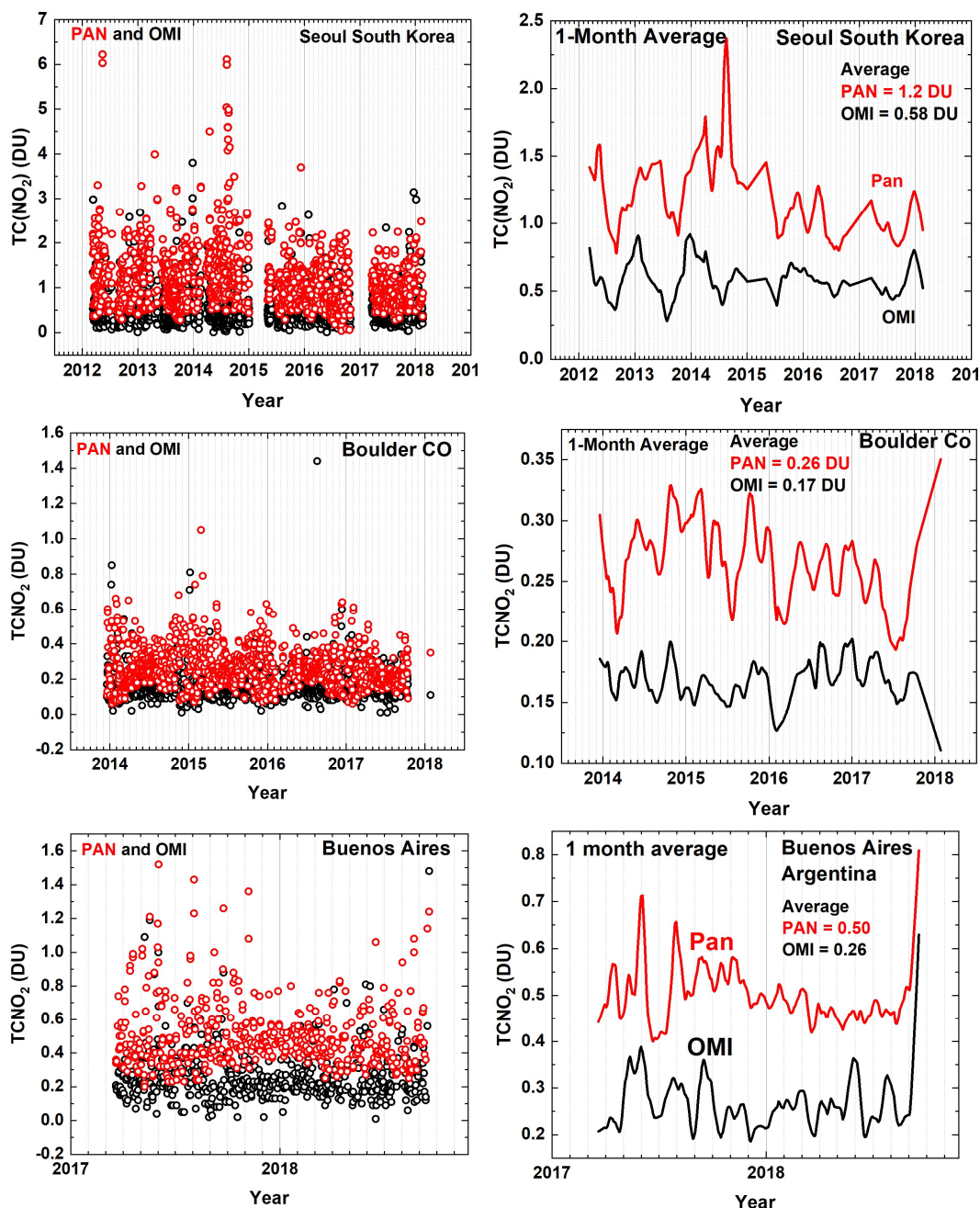


Fig. 5. PANDORA compared to OMI. Extended TCNO₂ overpass time series for Seoul South Korea, Boulder, Colorado, and Buenos Aires, Argentina (Raponi et al. 2017).



188 TCNO₂(PAN) comparisons with TCNO₂(OMI) from Mauna Loa Observatory (Fig. 4) are not those
189 that might be expected, since the PANDORA observations are in an area where there are almost no
190 automobile emissions and certainly no power plants, yet PAN > OMI and TCNO₂(PAN) values are large
191 enough so that the pollution values (0.18 DU) are well above the stratospheric values (approximately 0.1
192 DU). OMI, which mainly measures values over the clean ocean, has an average value of 0.1 DU. The
193 PANDORA values suggest upward airflow from the nearby circumferential ring road and resort areas. The
194 Mauna Loa TCNO₂ values do not show any correlation with the recent increased volcanic activity at Mt.
195 Kilauea after 2016. The calibration of the Mauna Loa PANDORA will be reviewed as part of a general data
196 quality assurance program that is starting with the most recently deployed PANDORA instruments.

197 An interesting inland site is near the very small town of Waterflow, New Mexico (Fig. 4), where
198 two power plants located near the PANDORA site ceased operation on December 30, 2013 (Lindenmaier
199 et al., 2014). According to a quote from AZCentral Newspaper (Tuesday 31 December 2013) “Three coal-
200 fired generators that opened in the 1960s near Farmington, N.M., closed Monday as part of a \$182 million
201 plan for Arizona Public Service Co. to meet environmental regulations, the utility reported”. The TCNO₂
202 data suggests that the actual shutdown occurred near October 15, 2013. After the shutdown, air quality
203 improved in the area with TCNO₂ decreasing from 0.4 DU to 0.28 DU. The remaining more efficient
204 generators continued to produce smaller NO₂ emissions. These were shut down at the end of 2016 with
205 little additional observed change in TCNO₂, since these boilers used NO₂ scrubbers (Dubey et al., 2018 in
206 preparation). A nearby highway (Route 64) about 2 km from the PANDORA site has little automobile
207 traffic.

208

209 Figures 4 and 5 show a variety of different sites, ranging from the Mauna Loa Observatory location
210 at 3.4 km (11,161 feet) on a relatively clean Hawaiian Island surrounded by ocean to a polluted landlocked
211 semi-arid site at Waterflow, New Mexico near a power plant. All the sites considered show a significant
212 underestimate of OMI TCNO₂. A summary of the monthly average underestimates is given in Tables 1 and
213 2. For some sites there is evident correlation between the two offset measurements. For example, the
214 PANDORA at NASA Headquarters in Washington DC tracks the OMI measurement quite well on a monthly
215 average basis. Other sites have only short periods of correlation.

216



217

Table 1 Average values of TCNO₂ for PANDORA and OMI from monthly averages in Figs. 4 and 5

| Location | PAN (DU) | OMI (DU) |
|------------------------|-------------|-------------|
| Mauna Loa Hawaii | 0.16 | 0.11 |
| NASA HQ Washington DC | 0.34 | 0.25 |
| Waterflow New Mexico | 0.32 | 0.18 |
| Seoul South Korea | 1.2 | 0.58 |
| Busan South Korea | 0.68 | 0.32 |
| Boulder Colorado | 0.27 | 0.17 |
| Buenos Aires Argentina | 0.50 | 0.26 |
| Average | 0.49 | 0.27 |

218

Table 2 Average values of TCNO₂ for PANDORA and OMI for additional sites

| Location | PAN (DU) | OMI (DU) |
|---|-------------|-------------|
| Essex Maryland | 0.30 | 0.28 |
| Baltimore Maryland | 0.45 | 0.27 |
| Fresno California | 0.42 | 0.17 |
| Denver La Casa Colorado | 0.68 | 0.19 |
| Gwangju Institute of Science and Technology (GIST) S. Korea | 0.42 | 0.20 |
| Hankuk University Foreign Studies (HUFS) South Korea | 0.61 | 0.51 |
| Average | 0.48 | 0.29 |

219

220 Table 2 contains a summary of sites that were part of short-term Discover-AQ campaigns in
 221 Maryland, Texas, California, and Colorado, and two longer-term sites in South Korea. Essex, Maryland is
 222 located on the Chesapeake Bay 10 km east of the center of Baltimore. The site is relatively clean (PAN =
 223 0.3 DU) compared to the center of Baltimore (PAN = 0.45 DU), while OMI measures about the same
 224 amounts for both sites (0.28 and 0.27 DU) because the OMI FOV is larger than the distance between the
 225 two sites. The Houston Texas site contains 7 months of data from January to July 2013 with widespread
 226 NO₂ pollution permitting PANDORA and OMI to measure the same average values even though PANDORA
 227 observes episodes on many days when TCNO₂ exceeds 1.5 DU for short periods at times not observed by
 228 OMI. Observations in the small city of Fresno, California were during January when agricultural sources of
 229 NO₂ were at a minimum (Almaraz, 2018), but automobile traffic in the center of Fresno was significant. In
 230 this situation, PANDORA recorded the effect of automobile traffic while OMI averaged the city of Fresno
 231 and surrounding fallow agricultural areas. The Denver La Casa location is in the center of the city in an
 232 area with high amounts of local automobile traffic and near the Cherokee power generating plant. The
 233 result is a high level of average pollution (0.42 DU) while OMI measures both the city center and the
 234 surrounding relatively clean plains areas. The HUFS South Korean site is southeast of Seoul in a fairly
 235 isolated valley. However, Seoul and its surrounding areas are a widespread transported source of pollution
 236 so that both PANDORA and OMI measure elevated TCNO₂ amounts. In contrast, the PANDORA GIST site is



237 on the outskirts of a small city in southwestern South Korea with significant traffic. The result is significant
238 amounts of localized TCNO₂ (PANDORA = 0.42) surrounded by areas that produce little NO₂ leading to
239 OMI observing a very clean 0.2 DU. The average of sites in the two tables are similar leading to ratios of
240 PAN/OMI of 1.8 and 1.7 respectively. The estimated 50% increase in OMI retrievals of TCNO₂ from using
241 the geometry-dependent reflectivity (Vasilkov, 2017) for the most polluted sites will narrow the
242 disagreement with PANDORA. For example, OMI Seoul TCNO₂ may become 0.87 DU (PANDORA = 1.2 DU)
243 and Buenos Aires 0.39 DU (PANDORA = 0.5 DU) still underestimating the amount of NO₂ pollution and
244 missing the significant diurnal variation.

245 The average percent differences between OMI and PANDORA shown in Fig. 6 are relatively
246 constant over time for each site with small changes over each multi-year observation period. Of the six
247 sites, only two of the sites have a statistically significant change in the percent difference (Seoul South
248 Korea and NASA HQ Washington DC) at the 2-standard deviation level (2σ). The average differences range
249 from 24% to 46%.

250 For the six sites shown, the average OMI underestimate of TCNO₂ is approximately a factor of 1.8
251 at the overpass time on a monthly average basis with occasional spikes that exceed this amount. The bias
252 values range from 1.1 to 3.6, with higher biases tending to be associated with higher TCNO₂ values. The
253 factor of 1.8 underestimate ignores the frequent large values of TCNO₂ at other times during the day (Fig.
254 7). In addition, averaging TCNO₂(PAN) over each entire day yields average values for the whole period that
255 are 10 to 20% higher than just averaging over midday values that matched the OMI overpass time. Aside
256 from the absolute magnitude, the short-term variations (over several months) are similar for both OMI
257 and PANDORA although mostly not correlated. If correlation coefficients r^2 are generated from linear fits
258 to scatter plots of TCNO₂ from OMI vs PANDORA, the correlation is mostly poor (Examples, r^2 =: Seoul
259 0.06, Mauna Loa 0.3 NASA HQ 0.7, see Figs. 4 and 5). Additional sites with shorter PANDORA time series
260 of TCNO₂ show similar behavior.

261 An alternate view of the differences between OMI and PANDORA is provided by forming the
262 percent differences of the daily TCNO₂ values (Fig. 6) in the form $100(\text{OMI} - \text{PAN})/\text{PAN}$. Also shown are
263 the average percent differences and the linear fit slopes in percent change per year of the percent
264 differences over the multi-year period. Of the six sites in shown in Fig. 6, two have statistically significant
265 slopes, Seoul South Korea 2.1 ± 0.5 %/Year and NASA Headquarters in Washington DC 3.4 ± 0.9 %/Year at
266 the 2σ level suggesting a significant area average increase in pollution compared to PANDORA's local
267 values.

268

269



270

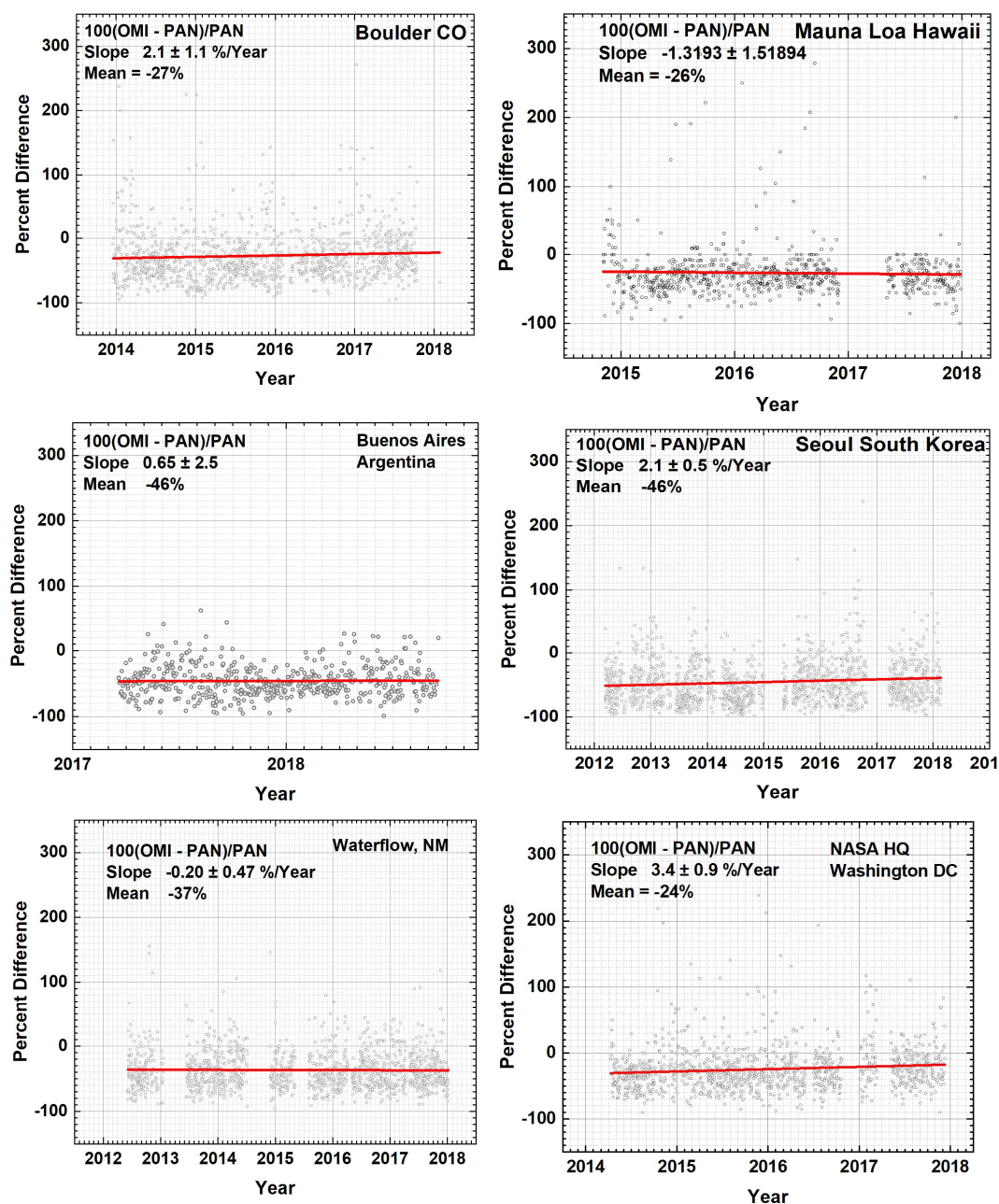


Fig. 6 Percent differences between OMI and PANDORA. The slopes are the absolute change in the percent difference. For example, the Boulder percent difference goes from -31% to -23% over 4 years.

271 **3.1 Diurnal Variation at NASA HQ Washington DC**



272 Figure 7 shows details of the daily diurnal variation of TCNO₂ on the roof of NASA Headquarters
 273 Washington, DC adjacent to a major cross town highway (I695) for every day during each month of 2015
 274 for local time vs DOY. The midday observing local standard time for OMI is marked for each graph.

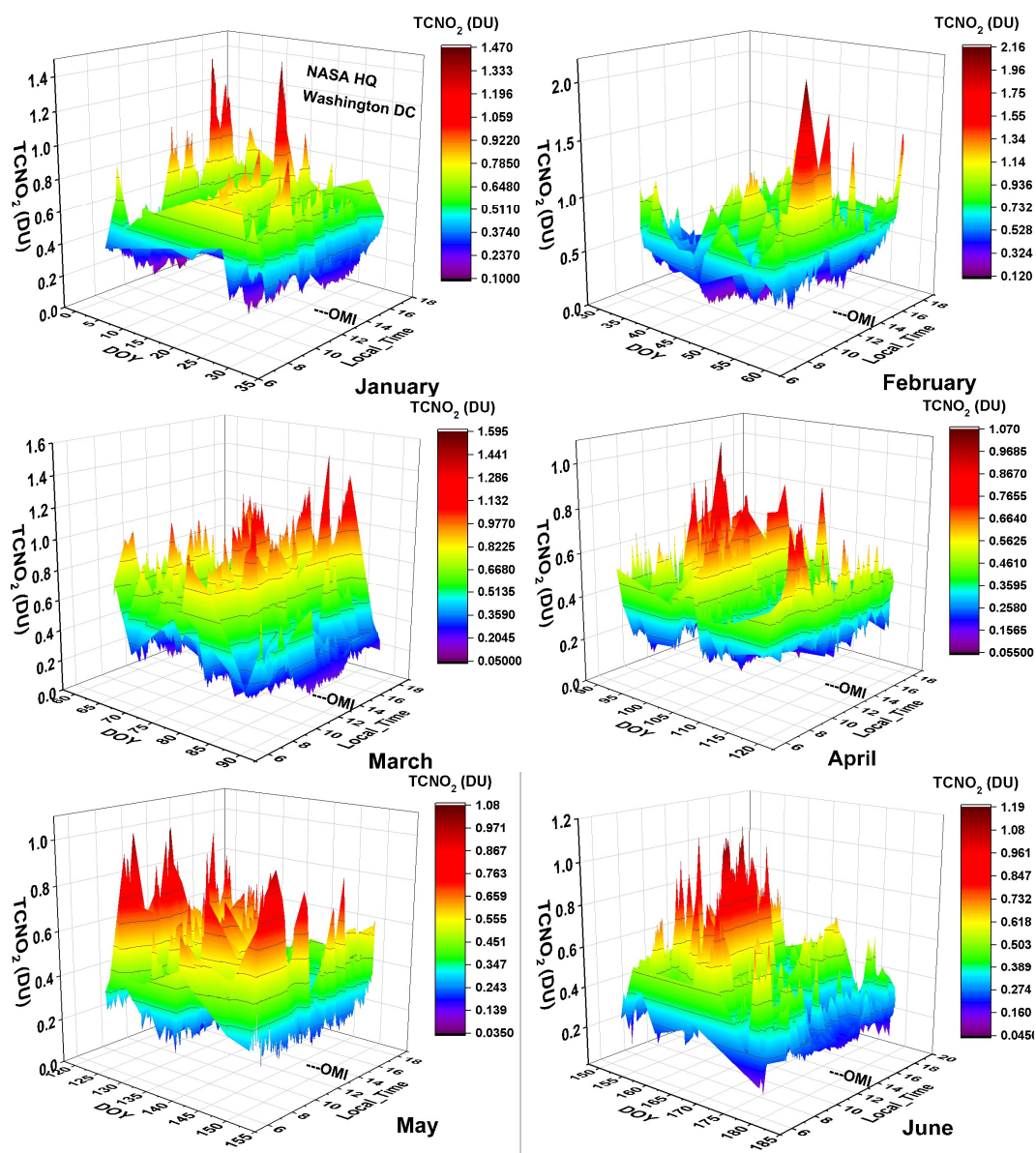


Fig. 7A. TCNO₂ diurnal variation (DU) from January to June, NASA Headquarters Washington, DC from January 2015 to June 2015. The approximate OMI overpass time near 13:30 hours is marked

275

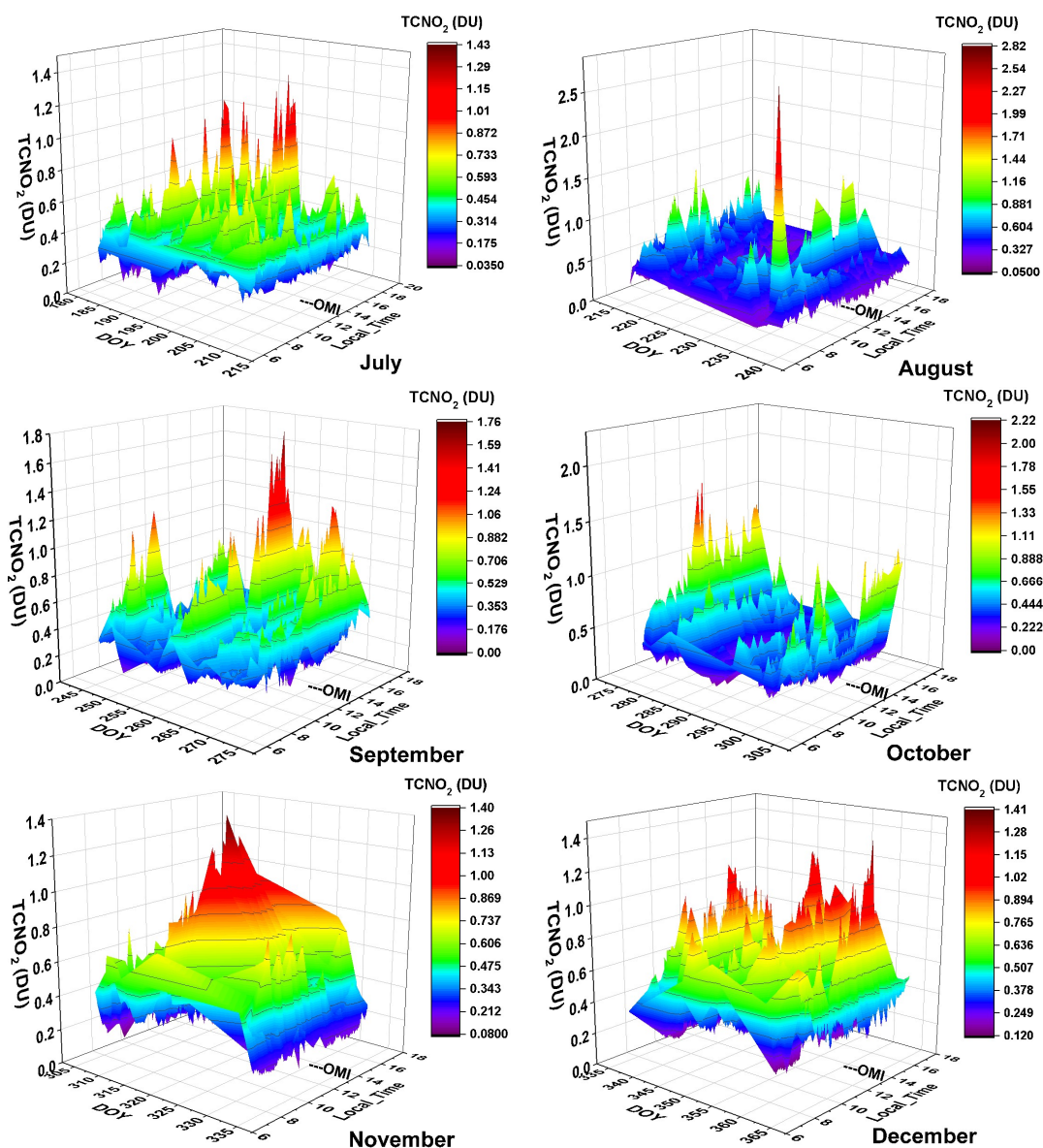


Fig. 7B TCNO₂ diurnal variation (DU) from July to December, NASA Headquarters Washington, DC from July 2015 to December 2015. The approximate OMI overpass time near 13:30 hours is marked

276

277 The amount of TCNO₂ is mostly from the adjacent highway and the surrounding urban area with
 278 heavy traffic. The relatively moderate TCNO₂ values (0.4 to 0.8 DU) are probably a testament to the
 279 effectiveness of catalytic converters mandatory on all US automobiles in such a high traffic area.

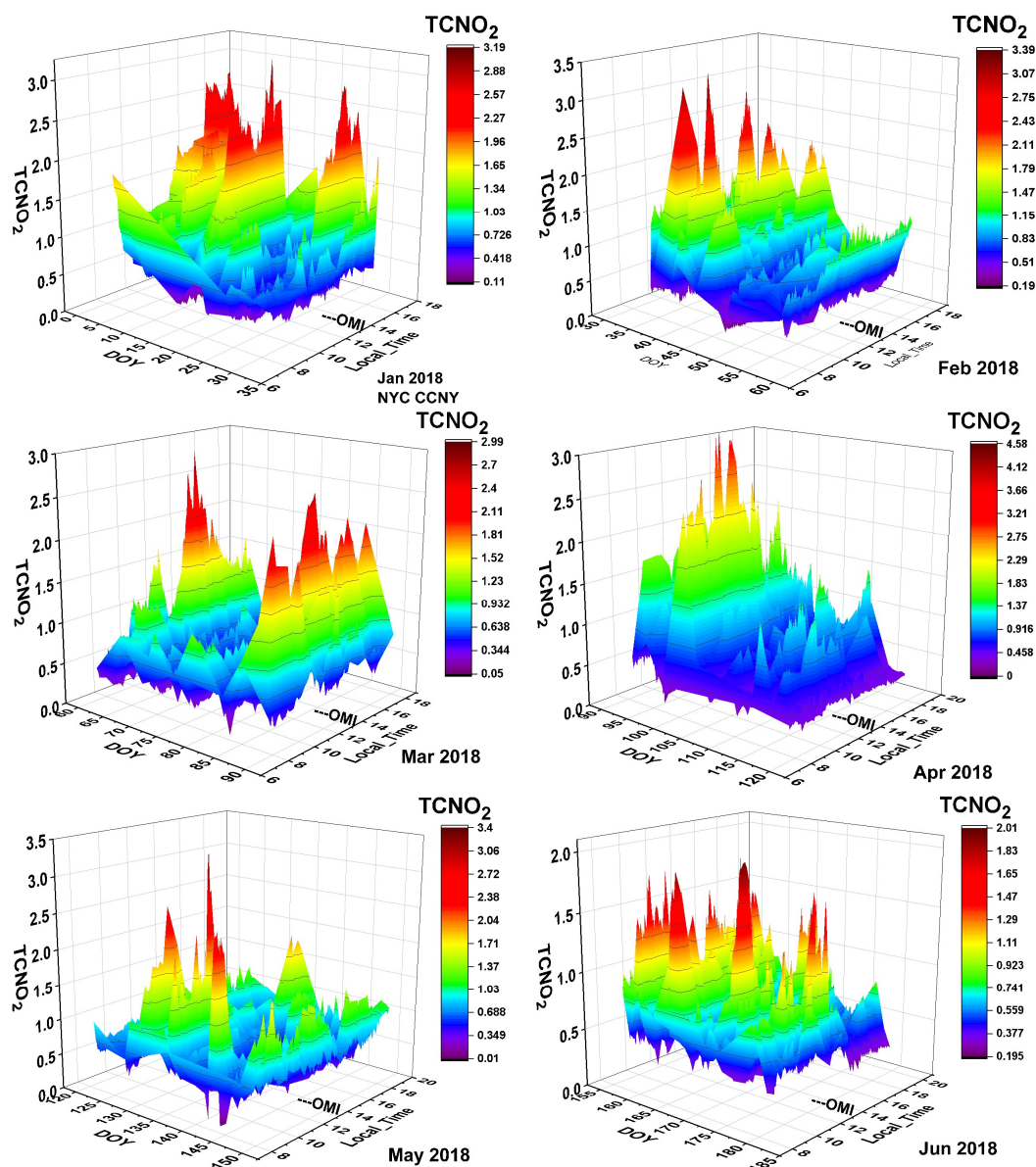


Fig. 8A TCNO₂ diurnal variation (DU) at CCNY in New York City January to June 2018. The approximate OMI overpass time near 13:30 hours is marked

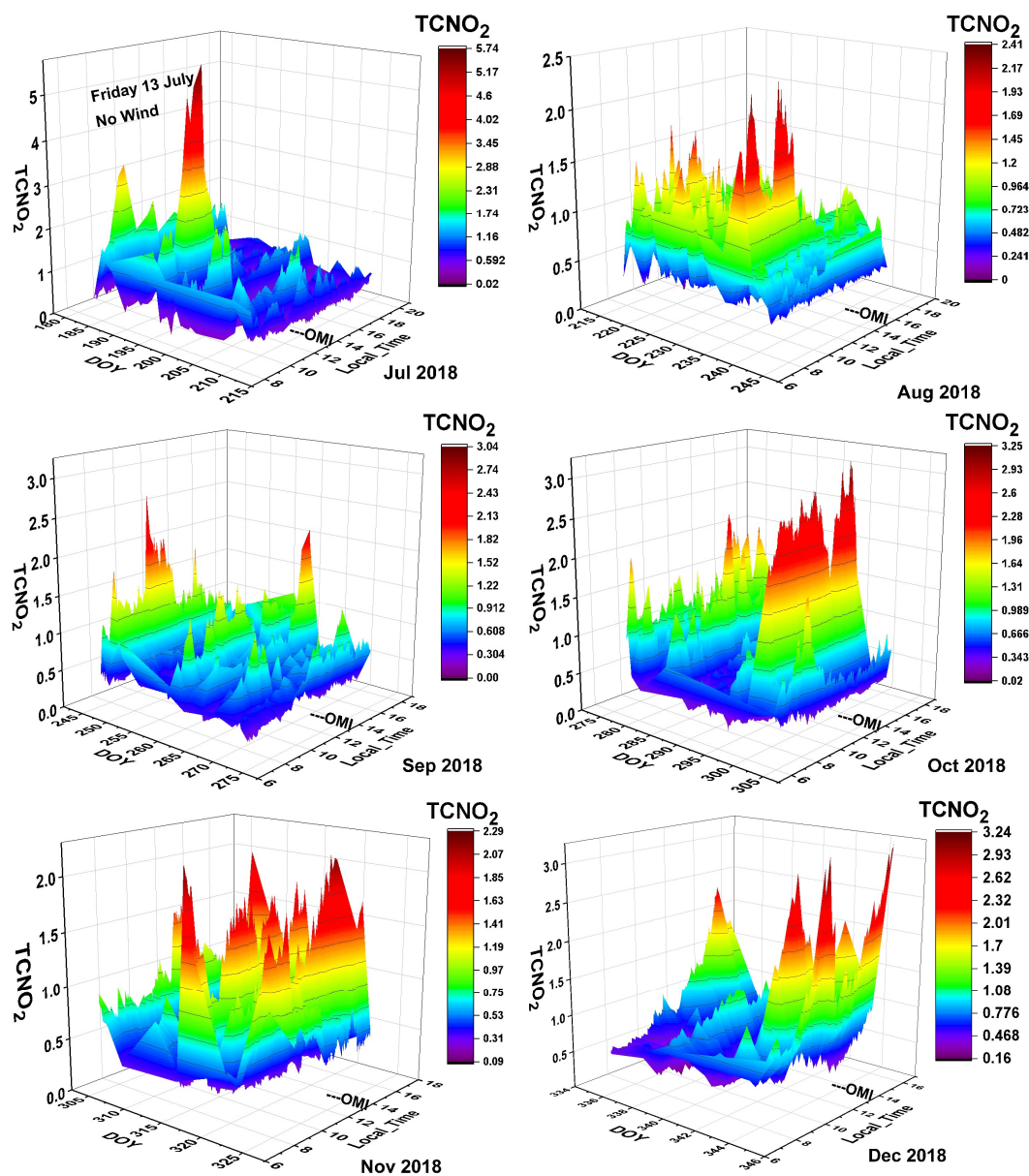


Fig. 8B TCNO₂ diurnal variation (DU) at CCNY in New York City July to December 2018. The peak near 5 DU occurs on 13 July 2018 between 11:20 and 12:30 EST. The approximate OMI overpass time near 13:30 hours is marked.

281

282 Figure 8 contains the daily TCNO₂ diurnal variability vs DOY for each month measured by a
 283 PANDORA from the roof of a building on the CCNY (City College of New York) campus in the middle of
 284 Manhattan in New York City (NYC). From the values shown, the pollution levels are quite high, rivaling the



285 pollution levels in Seoul, South Korea. OMI at its mid-day overpass time would detect some of the high-
286 level pollution events, but miss many others occurring mostly in the afternoon. There are a significant
287 number of days in all the months where the TCNO₂ levels appear to be low (e.g., blue color in July and
288 October), but the blue color still represents significant pollution levels (TCNO₂(PAN) > 0.5 DU) that are
289 small only compared to the peak values during the month (TCNO₂(PAN) > 1 DU). The highest amount of
290 TCNO₂ recorded during 2018 was about 5DU on 13 July 2018 from 11:20 and 12:30 EST (a time with very
291 light winds (1 km/hr) and moderate temperature (25°C). There were many smaller peaks between 2 and
292 3 DU throughout the year.

293 For both Washington DC (Fig. 7) and New York City (Fig. 8) there is strong day-to-day and month
294 to month variability that depends on the local weather and the amount of automobile traffic in the area.
295 High TCNO₂ events occur most often in the afternoon such that the OMI overpass near 13:30 would miss
296 most high TCNO₂ events. Poor air quality affecting respiratory health would be improperly characterized
297 by both the OMI average values being too low (Fig. 4) and by missing the extreme pollution events that
298 occur frequently in the late afternoon. The high value of TCNO₂ that occurred on 5 August (2.2 DU) at
299 07:45 EST for Washington DC is not a retrieval error (SZA less than 70°), but is a one-time anomaly in 2015
300 compared to more usual high values of 1.5 DU with an occasional spike to 2 DU.

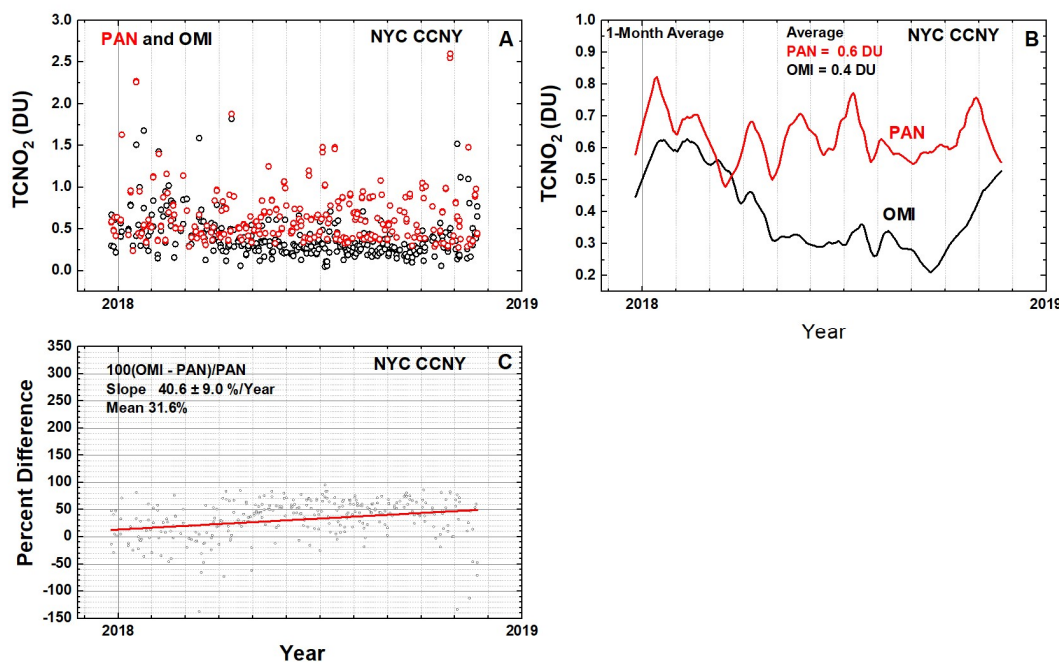


Fig. 9 TCNO₂ overpass time series for CCNY in Manhattan, New York City. Panel A: OMI overpass TCNO₂ (Black) compare with OMI (Red). Panel B: Monthly Lowess(0.08) fit to the daily overpass data. Panel C: Percent difference $100(\text{OMI} - \text{PAN})/\text{PAN}$ calculated from the data in Panel A



302 Similar daily diurnal variation graphs of TCNO₂ (Figs. 7 and 8) could be shown for each site.
303 However, the basic idea is the same for each site. OMI underestimates the amount of TCNO₂ because of
304 its large FOV and misses most of the peak events at other times of the day. For some sites, such as Busan
305 and Seoul, the peak values can reach 3 DU and above late in the afternoon, which are never seen by OMI
306 (Herman et al., 2018).

307 Figure 9 for CCNY is similar to the graphs in Figs. 4 – 6 showing the relative behavior between
308 PANDORA and OMI. However, there is a period in March 2018 when OMI TCNO₂ slightly exceeded that
309 measured by PANDORA. OMI with its large FOV may be seeing part of the chemically driven seasonal
310 variation, while PANDORA is seeing a nearly constant source driven amount mostly from automobile
311 traffic. For most days during 2018, PAN(TCNO₂) > OMI(TCNO₂) with the average value for PAN = 0.6 DU
312 and for OMI = 0.4 DU (Fig. 9 Panel B). The percent difference plot shows that there is a systematic increase
313 between PANDORA and OMI TCNO₂ from a value 10% to a value of 52%.

314 4.0 Summary

315 Examination of long-term TCNO₂ monthly average time series from OMI satellite and PANDORA
316 ground-based observations show that OMI systematically underestimates the amount of NO₂ in the
317 atmosphere by an average factor of 1.5 to 2 at the local OMI overpass time near the equator crossing time
318 of 13:30±1:30. The OMI underestimate is much larger than error estimates for TCNO₂ retrievals for either
319 PANDORA or OMI. In addition, the PANDORA diurnal time series for every day during a year at each site
320 (only two typical sites are shown in this paper) shows peaks in TCNO₂ that are completely missed by only
321 observing at mid-day. The result is that estimates of air quality related to health effects from OMI
322 observations are strongly underestimated almost everywhere as shown at all the sites with a long
323 PANDORA record. In comparisons to PANDORA, OMI data are mostly uncorrelated or weakly correlated
324 (e.g., Seoul correlation coefficient $r^2 = 0.06$, Mauna Loa $r^2 = 0.3$), while NASA HQ in Washington, DC shows
325 a correlation on a seasonal basis (NASA HQ $r^2 = 0.7$) suggesting a wide area coordinated source of NO₂
326 (most likely automobile traffic). The data from CCNY shows some correlation between the locations of the
327 peaks and troughs. Seven short term TCNO₂ time series were examined showing similar results (Table 1),
328 except when the pollution region is widespread as in the Seoul South Korea region. The conclusion is that
329 while OMI satellite TCNO₂ data are uniquely able to assess regional long-term trends in TCNO₂ and provide
330 a measure of the regional distribution of pollutants, the OMI data cannot properly assess local air quality
331 or the effect on human health over extended periods in urban or industrial areas. This will continue to be
332 the case, but to a lesser degree, when the OMI TCNO₂ data are improved by reprocessing with a new
333 geometry-dependent reflectivity (Vasilkov, 2017). The analysis shows that locating PANDORAs at polluted
334 sites could provide quantitative corrections for spatial and temporal biases that affect the determination
335 of local air quality from satellite data. To verify the proper operation of the various PANDORA instruments
336 a similar analysis for Total Column Ozone TCO was performed (see Appendix) and shows close agreement
337 between OMI and PANDORA, with the largest difference occurring for Mauna Loa Observatory at 3.4 km
338 altitude, where PANDORA misses the ozone between the surface and 3.4 km.

339



340

341 Appendix

342 **A1 Ozone** This section shows the corresponding PANDORA total column ozone (TCO) values
343 compared to OMI TCO for Busan South Korea (Fig. A1) that shows close agreement for the entire 2012 –
344 2017 period. The different fields of view for OMI and PANDORA have a much smaller effect because of
345 the greater spatial uniformity of stratospheric ozone compared to tropospheric NO₂. Additional sites are
346 summarized in Table A1. The largest TCO difference (15 DU or 5.6%) occurs for Mauna Loa Observatory
347 (Altitude = 3.4 km) compared to OMI (Average altitude = Sea Level). The close results show that the
348 PANDORA was working properly and pointing accurately at the sun.

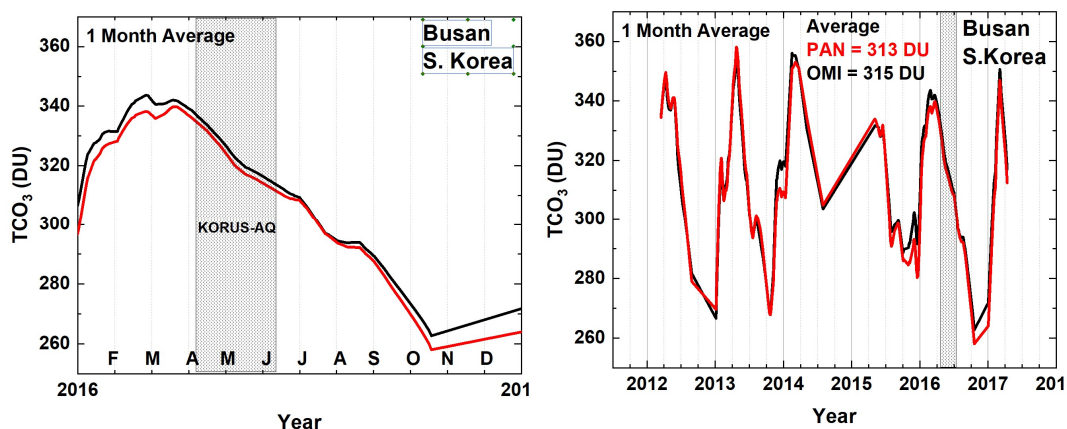


Fig. A1 Monthly average values of TCO for OMI and PANDORA at OMI overpass times for Busan South Korea

349

350



351

Table A1 Average values of TCO₃ for PANDORA and OMI

| Location | PAN (DU) | OMI (DU) | Percent Difference |
|--|-------------|-------------|-----------------------|
| Mauna Loa Observatory Hawaii (3.394 km)* | 254 | 269 | 5.6 |
| NASA HQ Washington DC (0.02 km) | 308 | 314 | 1.9 |
| Waterflow New Mexico (1.64 km) | 293 | 292 | 0.3 |
| Yonsei University Seoul South Korea (0.07 km) | 317 | 325 | 2.5 |
| Busan University Busan South Korea(0.03 km) | 313 | 315 | 0.6 |
| Boulder, Colorado (NOAA Bldg) (1.617 km) | 299 | 302 | 1.0 |
| Buenos Aires, Argentina (0.025 km) | 279 | 284 | 1.8 |
| Essex, Maryland (0.012 km) | 299 | 301 | 0.7 |
| Baltimore, Maryland (0.01 km) | 296 | 296 | 0.0 |
| Fresno, California (0.939 km) | 306 | 309 | 1.0 |
| Denver La Casa Colorado (1.6 km) | 292 | 294 | 0.7 |
| Gwangju Institute of Science and Technology (GIST) S. Korea (0.021 km) | 302 | 307 | 1.6 |
| Hankuk University Foreign Studies (HUFS) South Korea (0.04 km) | 318 | 326 | 2.5 |
| City College Manhattan New York City (0.04 km) | 316 | 325 | 2.8 |
| Average | 299 | 304 | 1.6 |

352

353 * OMI observes the sea level value of TCO₃

354

355

356

357

358

359

360

361 **Acknowledgement:** This project is supported by the Korea Ministry of Environment (MOE) as Public Technology
 362 Program based on Environmental Policy (2017000160001), by the Los Alamos National Laboratory's Laboratory
 363 Directed Research and Development program and by the NASA Pandora project managed by Dr. Robert
 364 Swap.



365 **References**

366 Almaraz, Maya, Edith Bai, Chao Wang, Justin Troudel, Stephen Conley, Ian Faloon and Benjamin Z.
367 Houlton, Agriculture is a major source of NO_x pollution in California, SCIENCE ADVANCES, 31,
368 DOI:10.1126/sciadv.aao3477, 2018.

369

370 Bechle, M. J.; Millet, D. B.; Marshall, J. D. Remote sensing of exposure to NO₂: Satellite versus ground-
371 based measurement in a large urban area. Atmos. Environ., 69, 345-353, 2013

372

373 Boersma, K. F., H. J. Eskes, E. J. Brinksma, Error analysis for tropospheric NO₂ retrieval from space, J.

374 Geophys. Res. Atmos., <https://doi.org/10.1029/2003JD003962>, 2004.

375 Boersma, K. F., Vinken, G. C. M., & Eskes, H. J., Representativeness errors in comparing chemistry
376 transport and chemistry climate models with satellite UV-Vis tropospheric column retrievals.

377 Geoscientific Model Development, 9(2), 875-898, 2016.

378 Choudhari, Sheetal Korde, Minal Chaudhary, Sachin Bagde, Amol R Gadbai and Vaishali Joshi, Nitric oxide
379 and cancer: a review, World Journal of Surgical Oncology 2013, 11:118,
380 <http://www.wjso.com/content/11/1/118>, 2013.

381

382 Cleveland, William S., *LOWESS: A program for smoothing scatterplots by robust locally weighted*
383 *regression. The American Statistician. 35 (1): 54. JSTOR 2683591. doi:10.2307/2683591, 1981.*

384

385 Goldberg, D. L., Saide, P. E., Lamsal, L. N., de Foy, B., Lu, Z., Woo, J.-H., Kim, Y., Kim, J., Gao, M., Carmichael,
386 G., and Streets, D. G.: A top-down assessment using OMI NO₂ suggests an underestimate in the NO_x
387 emissions inventory in Seoul, South Korea during KORUS-AQ, Atmos. Chem. Phys. Discuss.,
388 <https://doi.org/10.5194/acp-2018-678>, in review, 2018.

389

390 Herman, J., A. Cede, E. Spinei, G. Mount, M. Tzortziou, and N. Abuhassan, NO₂ column amounts from
391 ground-based Pandora and MFDOAS spectrometers using the direct-sun DOAS technique:
392 Intercomparisons and application to OMI validation, J. Geophys. Res., 114, D13307,
393 doi:10.1029/2009JD011848, 2009.

394

395 Herman, J.R., R.D. Evans, A. Cede, N.K. Abuhassan, I. Petropavlovskikh, and G. McConville, Comparison
396 of Ozone Retrievals from the Pandora Spectrometer System and Dobson Spectrophotometer in Boulder
397 Colorado, Atmos. Meas. Tech., 8, 3407-3418, 2015 doi:10.5194/amt-8-3407-2015

398

399 Herman, J., Spinei, E., Fried, A., Kim, J., Kim, J., Kim, W., Cede, A., Abuhassan, N., and Segal-Rozenhaimer,
400 M.: NO₂ and HCHO measurements in Korea from 2012 to 2016 from Pandora spectrometer instruments
401 compared with OMI retrievals and with aircraft measurements during the KORUS-AQ campaign, Atmos.
402 Meas. Tech., 11, 4583-4603, <https://doi.org/10.5194/amt-11-4583-2018>, 2018.

403



- 404 Ialongo, I., Herman, J., Krotkov, N., Lamsal, L., Boersma, K. F., Hovila, J., and Tamminen, J.: Comparison of
405 OMI NO₂ observations and their seasonal and weekly cycles with ground-based measurements in Helsinki,
406 Atmos. Meas. Tech., 9, 5203-5212, <https://doi.org/10.5194/amt-9-5203-2016>, 2016.
- 407
- 408 Kleipool, Q.L., M.R. Dobber, J.F. De Haan and P.F. Levelt, Earth Surface Reflectance Climatology from Three
409 Years of OMI Data, Journal of Geophysical Research, 113, doi:10.1029/2008JD010290, 2008.
- 410
- 411 Kollonige, D. E., Thompson, A. M., Josipovic, M., Tzortziou, M., Beukes, J. P., Burger, R., ... Laakso, L. (2018).
412 OMI satellite and ground-based Pandora observations and their application to surface NO₂ estimations
413 at terrestrial and marine sites. Journal of Geophysical Research: Atmospheres, 123, 1441–1459.
414 <https://doi.org/10.1002/2017JD026518>, 2018.
- 415
- 416 Lamsal, L. N., Krotkov, N. A., Celarier, E. A., Swartz, W. H., Pickering, K. E., Bucsela, E. J., Martin, R.
417 V., Philip, S., Irie, H., Cede, A., Herman, J., Weinheimer, A., Szykman, J. J., and Knepp, T. N.: Evaluation
418 of OMI operational standard NO₂ column retrievals using in situ and surface-based NO₂ observations,
419 Atmos. Chem. Phys. Discuss., 14, 14519-14573, doi:10.5194/acpd-14-14519-2014, 2014.
- 420
- 421 Lamsal, L. N., S. J. Janz, N. A. Krotkov, K. E. Pickering, R. J. D. Spurr, M. G. Kowalewski, C. P. Loughner, J. H.
422 Crawford, W. H. Swartz, and J. R. Herman, High-resolution NO₂ observations from the Airborne Compact
423 Atmospheric Mapper Retrieval and validation, J. Geophys. Res. Atmos., 122, 1953–1970,
424 doi:10.1002/2016JD025483, 2017
- 425
- 426 Levelt, P. F., Van den Oord, G. H. J., Dobber, M. R., Malkki, A., Visser, H., de Vries, J., Stammes, P., Lundell,
427 J. O. V., and Saari, H.: The Ozone Monitoring Instrument, IEEE T. Geosci. Remote, 44, 1093–1101,
428 doi:10.1109/tgrs.2006.872333, 2006.
- 429
- 430 Lindenmaier, Rodica, Manvendra K. Dubey, Bradley G. Henderson, Zachary T. Butterfield, Jay R. Herman,
431 Thom Rahn · S.-H. Lee, Multiscale observations of CO₂, (CO₂)-C-13, and pollutants at Four Corners for
432 emission verification and attribution, Proceedings of the National Academy of Sciences 06/2014;
433 111(23):8386-8391. DOI:10.1073/pnas.132188311, 2014
- 434
- 435 Liu, F., Beirle, S., Zhang, Q., Dörner, S., He, K., and Wagner, T.: NO_x lifetimes and emissions of cities and
436 power plants in polluted background estimated by satellite observations, Atmos. Chem. Phys., 16, 5283-
437 5298, <https://doi.org/10.5194/acp-16-5283-2016>, 2016.
- 438
- 439 O’Byrne, G., R. V. Martin, A. van Donkelaar, J. Joiner, and E. A. Celarier, Surface reflectivity from the Ozone
440 Monitoring Instrument using the Moderate Resolution Imaging Spectroradiometer to eliminate clouds:
441 Effects of snow on ultraviolet and visible trace gas retrievals, J. Geophys. Res., VOL. 115, D17305,
442 doi:10.1029/2009JD013079, 2010.
- 443
- 444 Marchenko, S., N. A. Krotkov, L. N. Lamsal, E. A. Celarier, W. H. Swartz, and E. J. Bucsela, Revising the
445 slant column density retrieval of nitrogen dioxide observed by the Ozone Monitoring Instrument, J.
446 Geophys. Res. Atmos., 120, 5670–5692, doi:10.1002/2014JD022913, 2015
- 447



- 448 Raponi, Marcelo, Cede, A, Santana Diaz, Daniel, Sanchez, R, A. Otero, L, O. Salvador, J, R. Ristori, P, Quel,
449 Eduardo. Total Column Ozone Measured In Buenos Aires Between March And November 2017, Using A
450 Pandora Spectrometer System. *Anales AFA*. 29(2), 46-50. 10.31527/analesafa.2018.29.2.46, 2018.
451
- 452 Torres, O., Bhartia, P. K., Jethva, H., and Ahn, C.: Impact of the ozone monitoring instrument row
453 anomaly on the long-term record of aerosol products, *Atmos. Meas. Tech.*, 11, 2701-2715,
454 <https://doi.org/10.5194/amt-11-2701-2018>, 2018.
455
- 456 Tzortziou, M.; Parker, O.; Lamb, B.; Herman, J.R.; Lamsal, L.; Stauffer, R.; Abuhassan, N. Atmospheric
457 Trace Gas (NO₂ and O₃) Variability in South Korean Coastal Waters, and Implications for Remote
458 Sensing of Coastal Ocean Color Dynamics. *Remote Sens.*, 10, 1587, ; doi:10.3390/rs10101587, 2018.
459
- 460 Vasilkov, A., Qin, W., Krotkov, N., Lamsal, L., Spurr, R., Haffner, D., Joiner, J., Yang, E.-S., and Marchenko,
461 S.: Accounting for the effects of surface BRDF on satellite cloud and trace-gas retrievals: a new approach
462 based on geometry-dependent Lambertian equivalent reflectivity applied to OMI algorithms, *Atmos.*
463 *Meas. Tech.*, 10, 333-349, <https://doi.org/10.5194/amt-10-333-2017>, 2017.
464
- 465 Zara, M., Boersma, K. F., De Smedt, I., Richter, A., Peters, E., van Geffen, J. H. G. M., Beirle, S.,
466 Wagner, T., Van Roozendaal, M., Marchenko, S., Lamsal, L. N., and Eskes, H. J.: Improved slant column
467 density retrieval of nitrogen dioxide and formaldehyde for OMI and GOME-2A from QA4ECV:
468 intercomparison, uncertainty characterization, and trends, *Atmos. Meas. Tech.*, 11, 4033-4058,
469 <https://doi.org/10.5194/amt-11-4033-2018>, 2018.
470



- 471 Figure Captions
- 472 Fig 1 Diurnal variation of TCNO₂ measured at Pusan University in Busan South Korea
- 473 Fig. 2. Monthly average values of TCNO₂ for OMI and PANDORA at OMI overpass times
- 474 Fig. 3 Extended time series for Busan. Left Panel: individual matching PANDORA and OMI data
475 points for the overpass time ± 6 minutes. Right Panel: monthly averages.
- 476 Fig. 4. PANDORA compared to OMI. Extended TCNO₂ overpass time series for Mauna Loa
477 Observatory, Hawaii, NASA Headquarters, Washington DC, and Waterflow, New Mexico.
- 478 Fig. 5. PANDORA compared to OMI. Extended TCNO₂ overpass time series for Seoul South Korea,
479 Boulder, Colorado, and Buenos Aires, Argentina (Raponi et al. 2018).
- 480 Fig. 6 Percent differences between OMI and PANDORA. The slopes are the absolute change in the
481 percent difference. For example, the Boulder percent difference goes from -31% to -23% over 4 years.
- 482 Fig. 7A TCNO₂ diurnal variation (DU) from January to June, NASA Headquarters Washington, DC
483 from January 2015 to June 2015. The approximate OMI overpass time near 13:30 hours is marked.
- 484 Fig. 7B TCNO₂ diurnal variation (DU) from July to December, NASA Headquarters Washington, DC from
485 July 2015 to December 2015. The approximate OMI overpass time near 13:30 hours is marked
- 486 Fig. 8A TCNO₂ diurnal variation (DU) at CCNY in New York City January to June 2018. The approximate
487 OMI overpass time near 13:30 hours is marked.
- 488 Fig. 8B TCNO₂ diurnal variation at CCNY in New York City July to December 2018. The peak near 5 DU
489 occurs on 13 July 2018 between 11:20 and 12:30 EST. The approximate OMI overpass time near 13:30
490 hours is marked.
- 491 Fig. 9 TCNO₂ overpass time series for CCNY in Manhattan, New York City. Panel A: OMI overpass
492 TCNO₂ (Black) compare with OMI (Red). Panel B: Monthly Lowess(0.08) fit to the daily overpass
493 data. Panel C: Percent difference $100(\text{OMI} - \text{PAN})/\text{PAN}$ calculated from the data in Panel A
- 494 Fig. A1 Monthly average values of TCO for OMI and PANDORA at OMI overpass times for Busan South
495 Korea

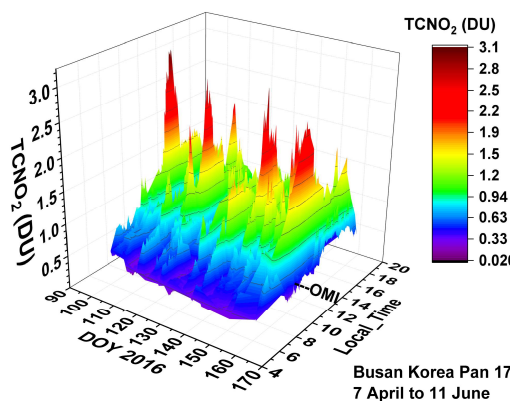


Fig 1 Diurnal variation of TCNO₂ measured at Pusan University in Busan South Korea

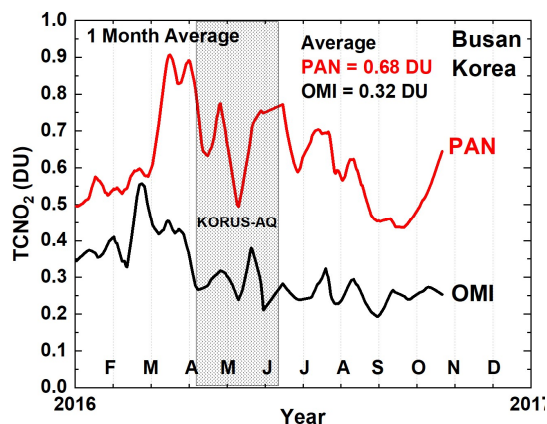


Fig. 2. Monthly average values of TCNO₂ for OMI and PANDORA at OMI overpass times

496

497

498

499 **FIGURE 1**

500

501

FIGURE 2

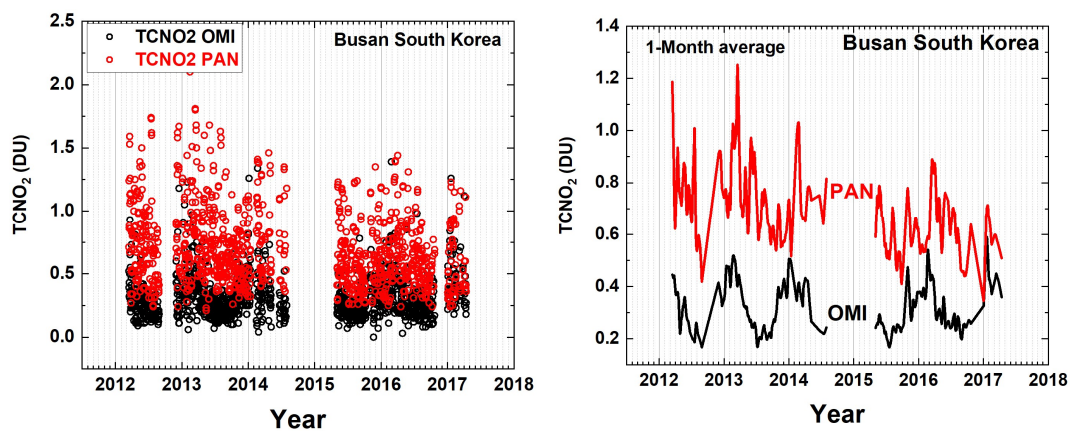


Fig. 3 Extended time series for Busan. Left Panel: individual matching PANDORA and OMI data points for the overpass time ± 6 minutes. Right Panel: monthly averages.

502

503

504 **FIGURE 3**

505

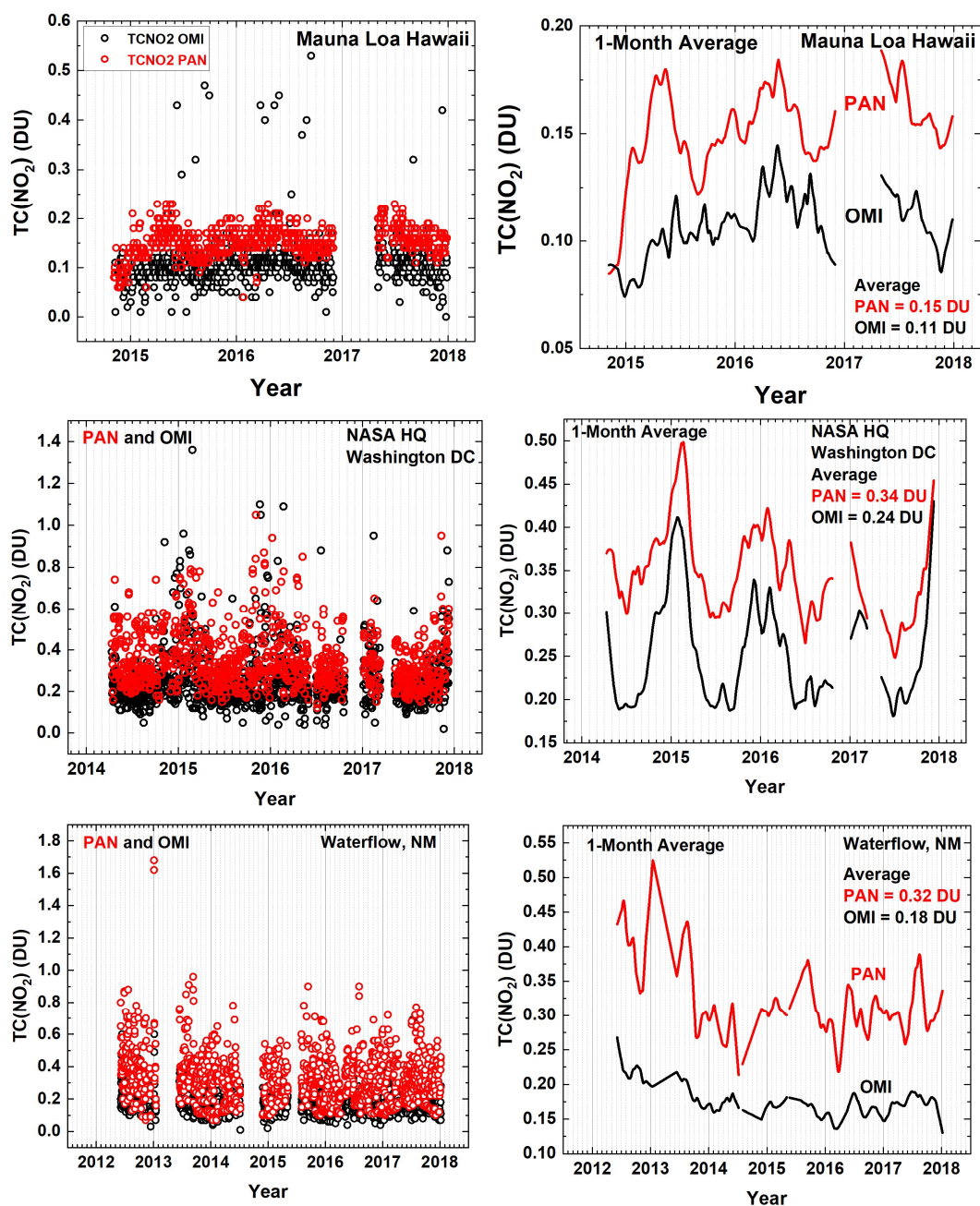


Fig. 4. PANDORA compared to OMI. Extended TCNO₂ overpass time series for Mauna Loa Observatory, Hawaii, NASA Headquarters, Washington DC, and Waterflow, New Mexico.

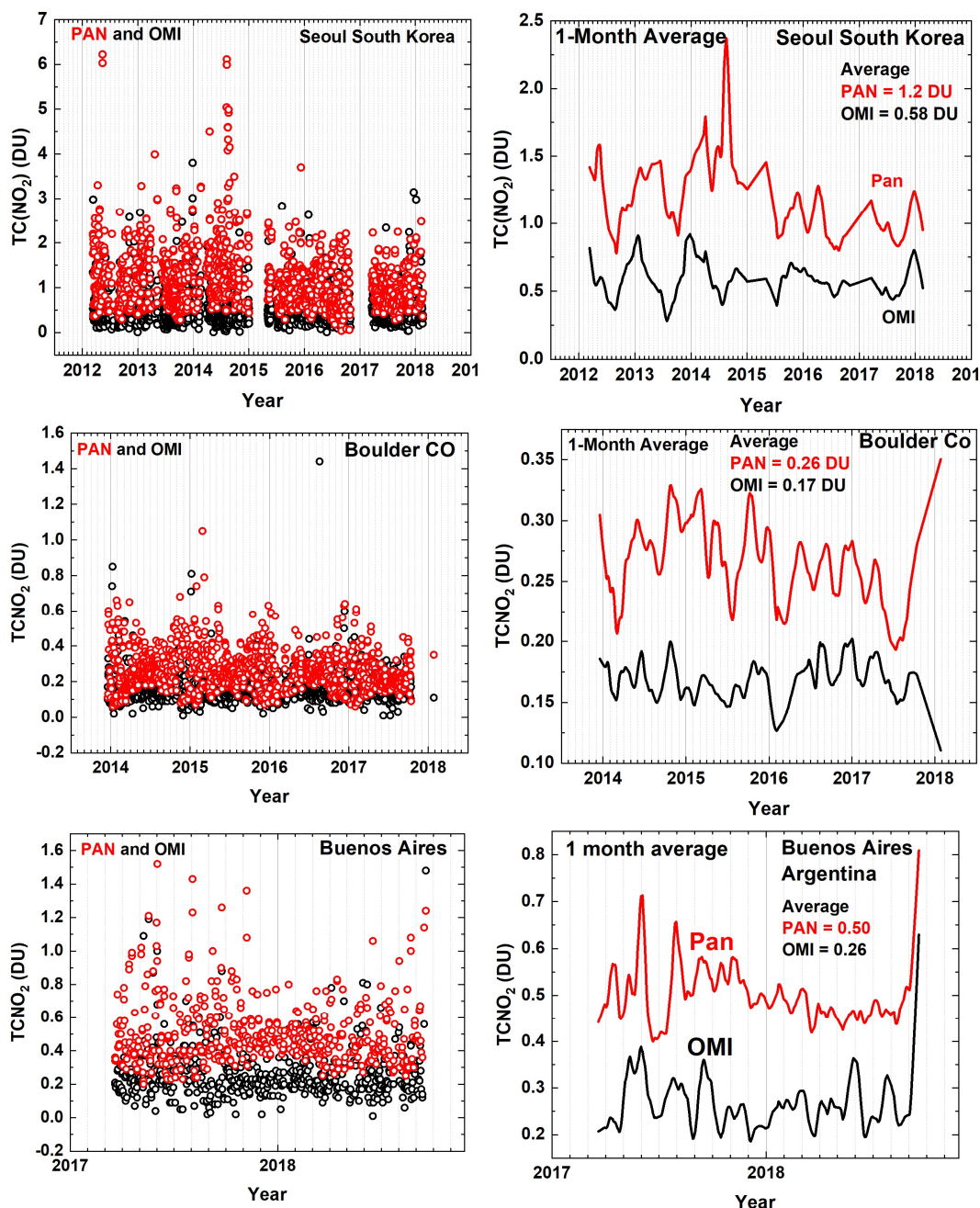


Fig. 5. PANDORA compared to OMI. Extended TCNO₂ overpass time series for Seoul South Korea, Boulder, Colorado, and Buenos Aires, Argentina (Raponi et al. 2017).



508

509

510

511

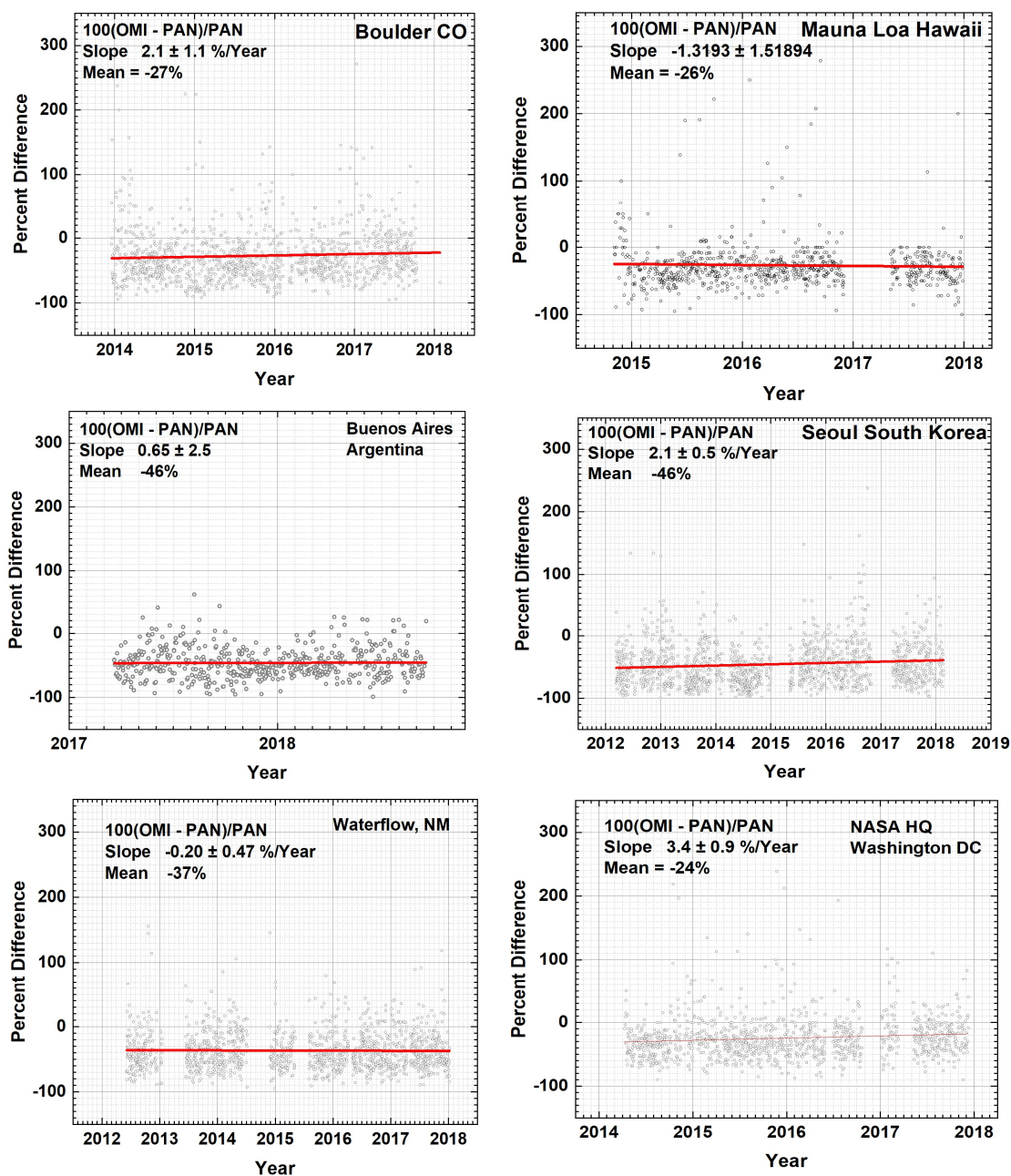


Fig. 6 Percent differences between OMI and PANDORA. The slopes are the absolute change in the percent difference. For example, the Boulder percent difference goes from -31% to -23% over 4 years.

FIGURE 6



512

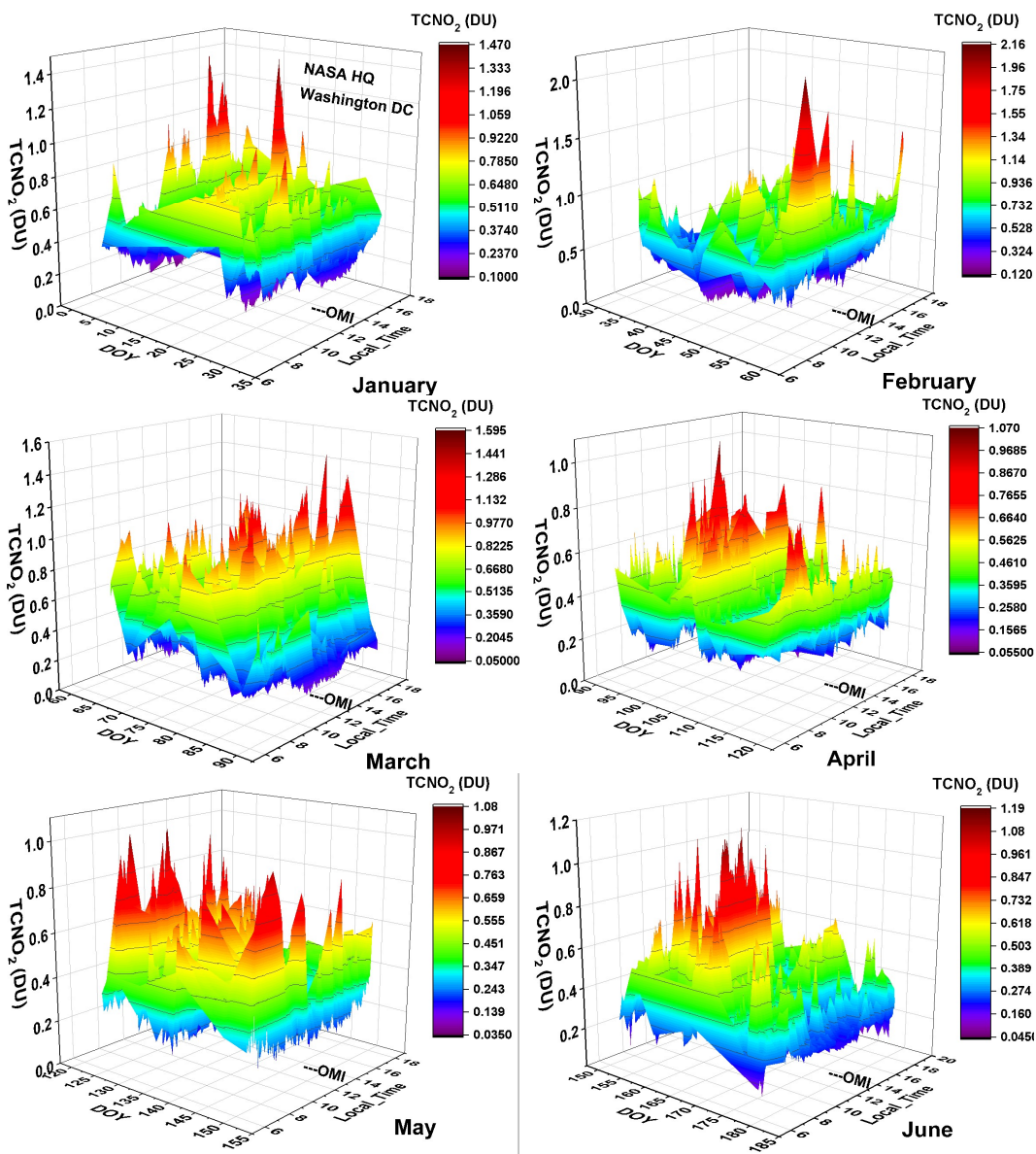


Fig. 7A TCNO₂ diurnal variation (DU) from January to June, NASA Headquarters Washington, DC from January 2015 to June 2015. The approximate OMI overpass time near 13:30 hours is marked

513

FIGURE 7A

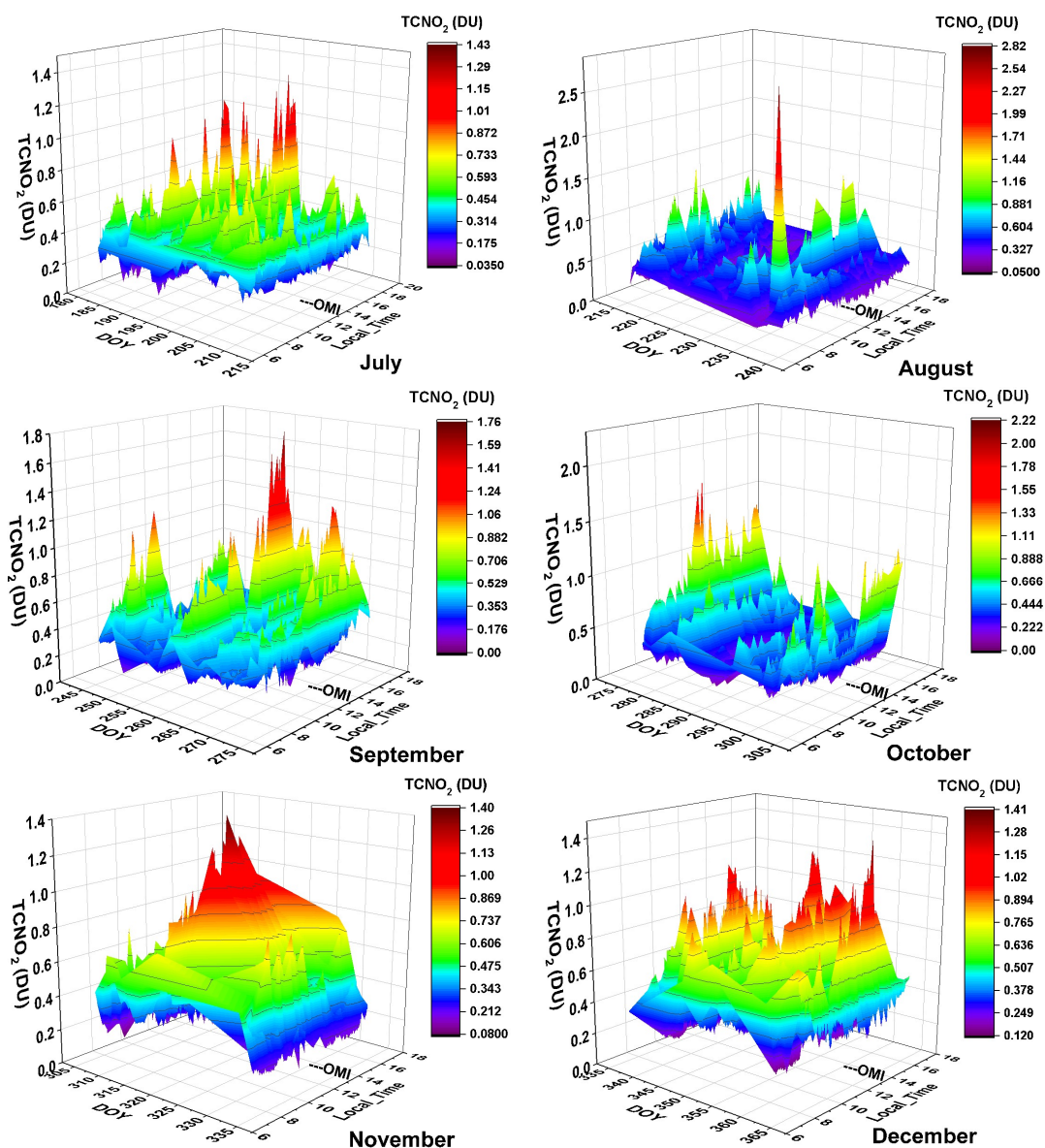


Fig. 7B TCNO₂ diurnal variation (DU) from July to December, NASA Headquarters Washington, DC from July 2015 to December 2015. The approximate OMI overpass time near 13:30 hours is marked

514

515 **FIGURE 7B**

516

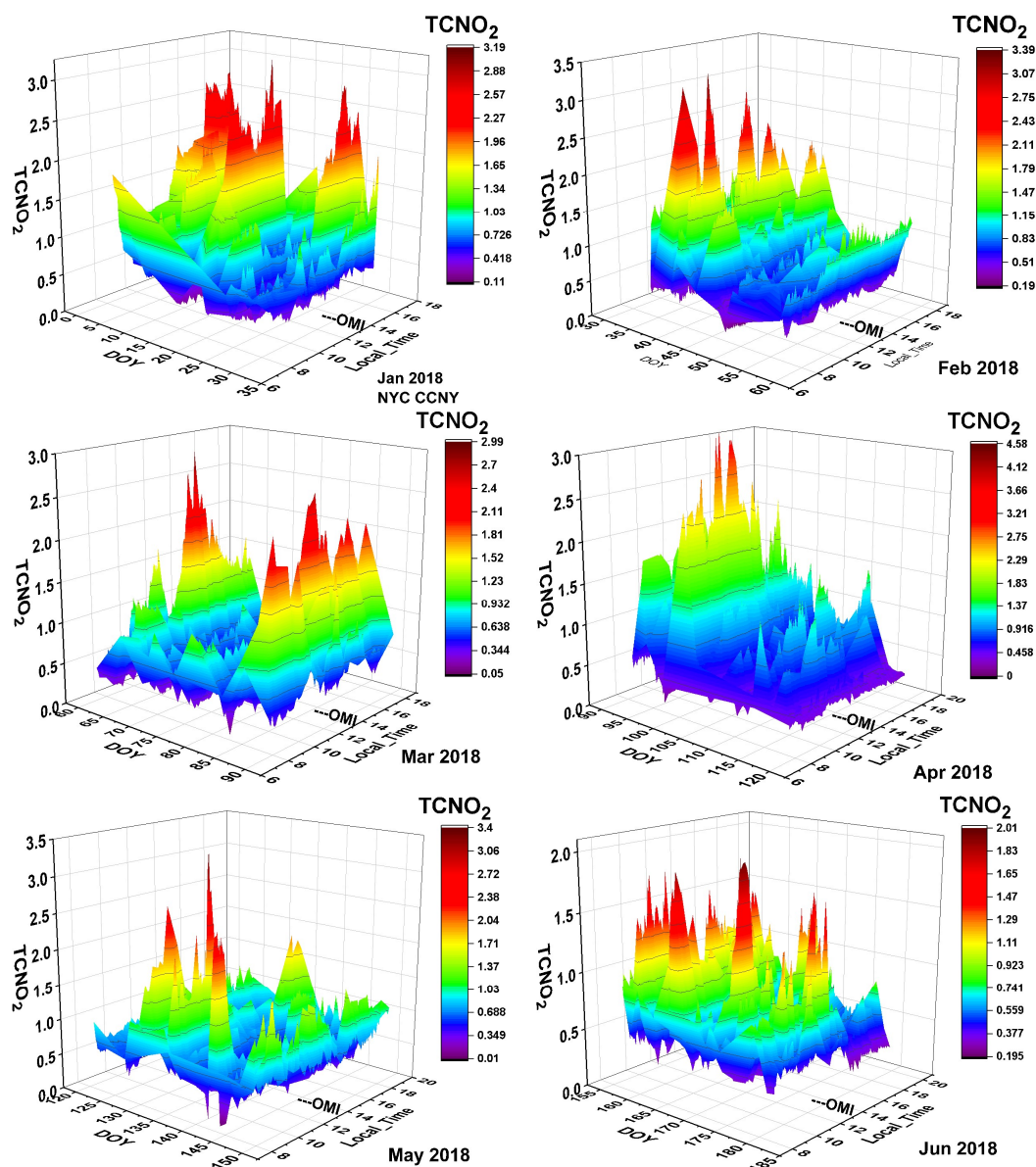


Fig. 8A TCNO₂ diurnal variation (DU) at CCNY in New York City January to June 2018. The approximate OMI overpass time near 13:30 hours is marked

517

518 **Figure 8A**

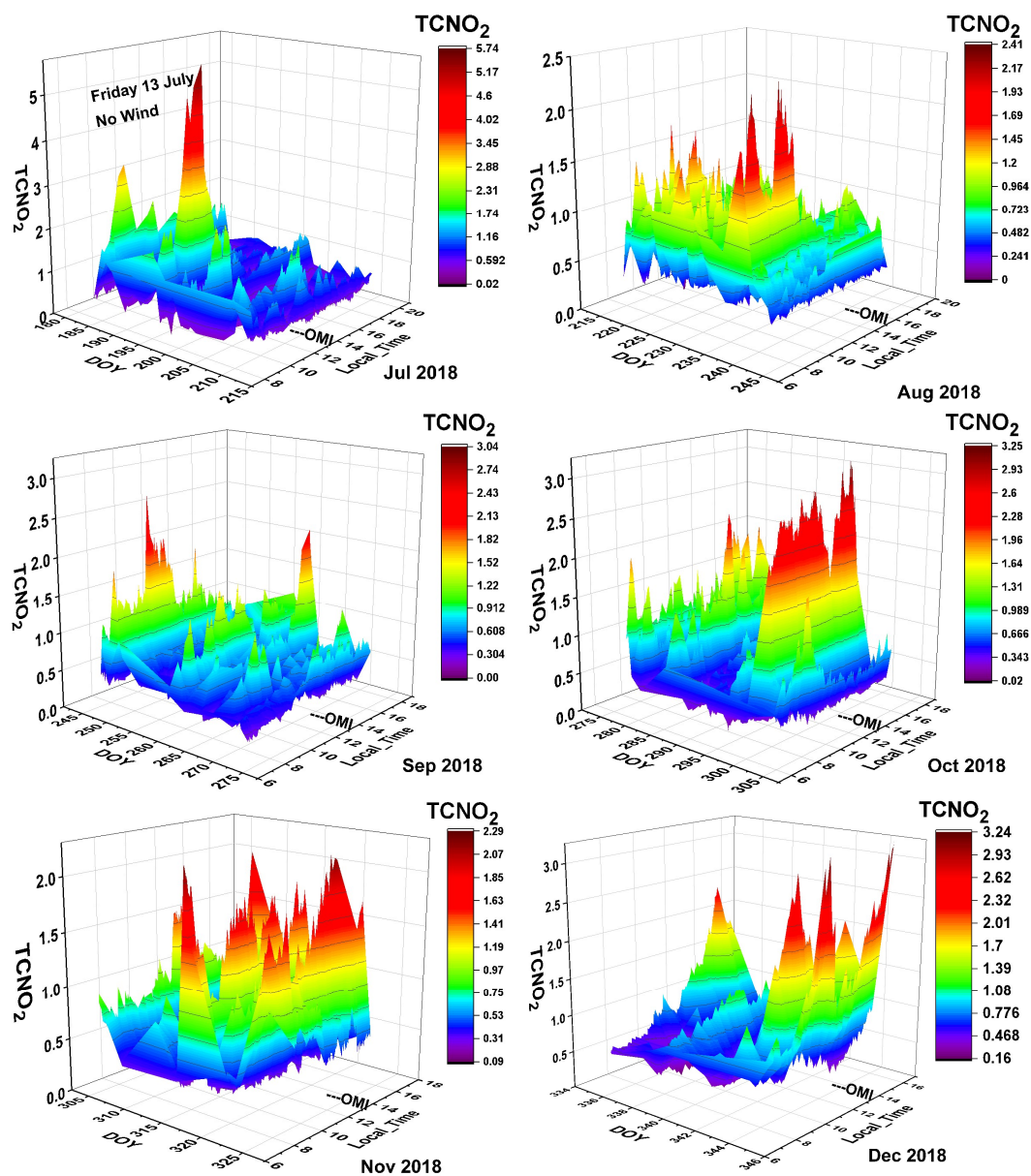


Fig. 8B TCNO₂ diurnal variation (DU) at CCNY in New York City July to December 2018. The peak near 5 DU occurs on 13 July 2018 between 11:20 and 12:30 EST. The approximate OMI overpass time near 13:30 hours is marked.

519

520 **Figure 8B**

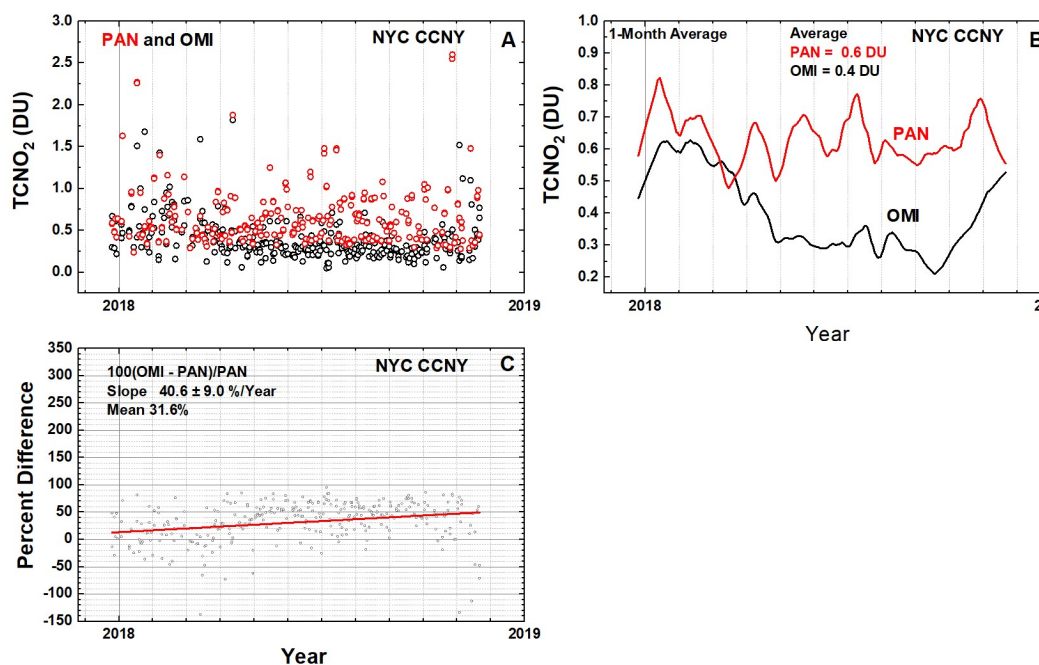


Fig. 9 TCNO₂ overpass time series for CCNY in Manhattan, New York City. Panel A: OMI overpass TCNO₂ (Black) compare with OMI (Red). Panel B: Monthly Lowess(0.08) fit to the daily overpass data. Panel C: Percent difference $100(OMI - PAN)/PAN$ calculated from the data in Panel A

521

522 **Figure 9**

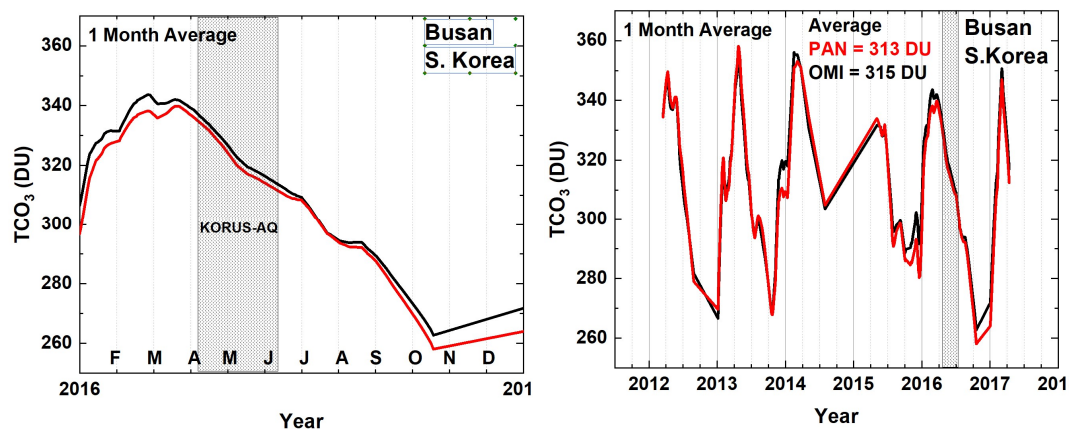


Fig. A1 Monthly average values of TCO₃ for OMI and PANDORA at OMI overpass times for Busan South Korea

523

524

525 **FIGURE A1**